

# Transformer Transforms Salient Object Detection and Camouflaged Object Detection

Yuxin Mao<sup>‡</sup>, Jing Zhang<sup>‡</sup>, Zhexiong Wan, Yuchao Dai\*,  
Aixuan Li, Yunqiu Lv, Xinyu Tian, Deng-Ping Fan and Nick Barnes

**Abstract**—The transformer networks, which originate from machine translation, are particularly good at modeling long-range dependencies within a long sequence. Currently, the transformer networks are making revolutionary progress in various vision tasks ranging from high-level classification tasks to low-level dense prediction tasks. In this paper, we conduct research on applying the transformer networks for salient object detection (SOD). Specifically, we adopt the dense transformer backbone for fully supervised RGB image based SOD, RGB-D image pair based SOD, and weakly supervised SOD within a **unified** framework based on the observation that the transformer backbone can provide accurate structure modeling, which makes it powerful in learning from weak labels with less structure information. Further, we find that the vision transformer architectures do not offer direct spatial supervision, instead encoding position as a feature. Therefore, we investigate the contributions of two strategies to provide stronger spatial supervision through the transformer layers within our unified framework, namely deep supervision and difficulty-aware learning. We find that deep supervision can get gradients back into the higher level features, thus leads to uniform activation within the same semantic object. Difficulty-aware learning on the other hand is capable of identifying the hard pixels for effective hard negative mining. We also visualize features of conventional backbone and transformer backbone before and after fine-tuning them for SOD, and find that transformer backbone encodes more accurate object structure information and more distinct semantic information within the lower and higher level features respectively. As an extension, we also apply our model to camouflaged object detection (COD) and achieve similar observations as the above three SOD related tasks. Extensive experimental results on various SOD and COD tasks illustrate that transformer networks can transform salient object detection and camouflaged object detection, leading to new benchmarks for each related task. The source code and experimental results are publicly available via our project page: <https://github.com/fupiao1998/TrasformerSOD>.

**Index Terms**—Vision Transformer, Salient Object Detection, Camouflaged Object Detection.

## 1 INTRODUCTION

Visual salient object detection [1], [2], [3], [4], [5], [6], [7] aims to localize the regions of an image that attract human attention. For static image based salient object detection, researchers mostly consider one of two fully supervised tasks, namely RGB image based salient object detection [1], [2] and RGB-D image pair based salient object detection [3], [4]. To reduce the labeling effort, several weakly supervised salient object detection models have been proposed to learn saliency with image-level supervision [6], scribble supervision [5] or learn saliency directly from noisy labeling [8], [9].

Before the deep learning revolution, conventional salient object detection models [10], [11] used handcrafted features as shown in Fig. 2, which define saliency as contrast [12] between each pixel (or superpixel) and the other pixels (or superpixels). In this way, the receptive field of the conventional handcrafted-feature based models is the entire image, which is global context as shown in Fig. 1, where saliency of the pixel colored in yellow depends on all the other pixels. However, the less representative

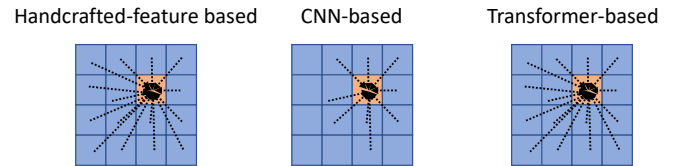


Fig. 1. Receptive field comparison of conventional handcrafted-feature based salient object detection models, CNN-based models and Transformer-based models.

handcrafted-feature limited their performance. The deep convolutional neural network (CNN) based salient object detection models [1], [2], [13], [14] achieve significant performance improvement compared with those handcrafted-feature based techniques with more sophisticated features extracted from the deep network.

The conventional deep CNN based SOD network usually includes two main parts: an encoder to extract different levels of features, and a decoder to aggregate features from different levels of the network for finer prediction. The encoder part is adopted from the trained backbone network on ImageNet, e.g., VGG [15], ResNet [16], and the most effort for SOD models has been put on designing an effective decoder for feature aggregation [1], [2], [17].

Conventional backbones have gradually larger receptive fields with the deeper layers. The main issue with these backbone networks is that the larger receptive field is obtained with the loss of structure information as a sacrifice. This is the reason for

- Yuxin Mao, Zhexiong Wan, Yuchao Dai, Aixuan Li, Yunqiu Lv and Xinyu Tian are with School of Electronics and Information, Northwestern Polytechnical University, China.
- Jing Zhang and Nick Barnes are with School of Computing, Australian National University.
- Deng-Ping Fan is with the CS, Nankai University, Tianjin, China.
- ‡: Equal contributions.
- Corresponding author: Yuchao Dai (Email: daiyuchao@nwpu.edu.cn).

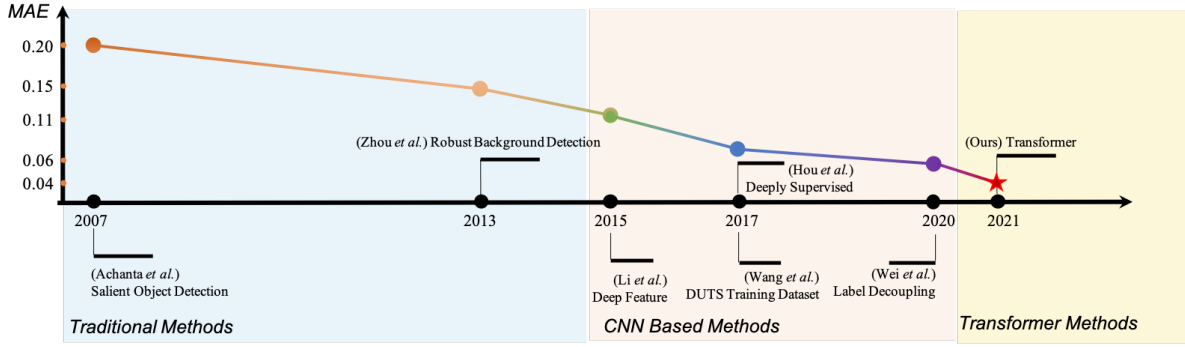


Fig. 2. A simplified timeline of salient object detection models, where the y-axis shows the mean absolute error (MAE) of related models on the DUT testing dataset [11]. Initially, Itti *et al.* [18] defined saliency detection as fixation prediction to predict the fixation points of salient objects. Then, Achanta *et al.* [19] introduced saliency detection as binary segmentation task to produce a segmentation map instead of a fixation map. The first CNN based deep saliency model [20] appeared in 2015, which replaced the handcrafted features with deep features. We introduce transformer backbone based salient object detection model with significantly improved model performance.

incorporating an additional complicated decoder. Note that, once the information is lost, it will not be fully recovered. Further, although the theoretical receptive field of a CNN covers the entire image [21], many studies have shown that the actual receptive field of a CNN is much smaller than the theoretical receptive field. In this way, a network with a larger receptive field without losing fine-grained information can be beneficial for context based tasks, *e.g.*, salient object detection, to achieve effective context modeling.

Researchers found that the “Transformer” [22] has great potential to solve the limited receptive field issue in vision tasks. The advantage of the “Transformer” lies in the use of self-attention to capture global contextual information to establish a long-range dependency as shown in Fig. 1, and it can extract more meaningful features. Different from convolutional neural networks that focus on a small patch of the image with a sliding window wise convolution operation, the transformer network [22] performs global context modeling. Inspired by [23], [24] and the accurate structure modeling ability of transformer, we present a “unified” transformer backbone based SOD network to achieve fully-supervised RGB image based SOD, RGB-D image pair based SOD and weakly-supervised RGB image based SOD with scribble annotation, leading to three new benchmark models as shown in Table 1 and Table 3.

We also observe that the positional encodings of vision transformer is less effective in modeling the accurate “spatial” information for dense prediction tasks. Then we investigate deep supervision and difficulty-aware learning within the transformer backbone as shown in Fig. 3 (the generation of the five different predictions  $s_l$  and confidence maps  $c_l$  are introduced in Section 3.3.1). We find that deep supervision can get gradients back into the higher level features, thus leads to uniform activation within the same semantic object as shown in Fig. 13. Difficulty-aware learning on the other hand is capable of identifying the hard pixels for effective hard negative mining (Fig. 3 “ $c_l$ ”). Further, we visualize the features of the CNN backbone and the transformer backbone in second row of Fig. 3, and find that transformer backbone encodes more accurate object structure information and more distinct semantic information within the lower and higher level features respectively.

Our main contributions are: 1) we introduce a unified transformer backbone [24] based network for three static image based salient object detection tasks, and one RGB image based camou-

flaged object detection task. We discover the superior performance of the transformer backbone for accurate structure modeling, which makes it powerful in learning from weak annotations; 2) we investigate two strategies, namely deep supervision and difficulty-aware learning, and illustrate the effectiveness of them for transformer backbone based frameworks to generate stronger spatial supervision; 3) we compare feature of CNN backbones and transformer backbones and find that the superior performance of transformer backbones mostly lies in the accurate structure and semantic information encoding with the long-range dependency modeling mechanism.

## 2 RELATED WORK

In this section, we will introduce the existing SOD and COD models, and recent work on transformer network.

### RGB Image based Fully Supervised Salient Object Detection:

As discussed above, existing fully supervised RGB image based salient object detection models [1], [2], [13], [14], [17], [25] mainly focus on designing effective decoder to achieve high-low level feature aggregation. Wu *et al.* [1] proposes a “Stacked Cross Refinement Network”, and uses the interaction between the edge module and the detection module to optimize the two tasks at the same time. We *et al.* [2] introduces an adaptive selection of complementary information when aggregating multi-scale features, and presents a structure-aware loss function, which solves the problem of differences in multi-scale features during fusion. Qin *et al.* [26] uses multiple supervisions and high-quality boundaries to guide the encoder, decoder and residual refinement module to gradually optimize the saliency prediction to obtain a more refined segmentation. [27] integrates the information of adjacent layers, and integrates multi-scale information to retain the internal consistency of each category (salient foreground or non-salient background).

### RGB Image based Weakly Supervised Salient Object De-

**tection:** The weakly supervised saliency models [5], [6], [9], [28], [29], [30] learn saliency from easy-to-obtain weak labels, including image-level labels [6], [28], noisy labels [8], [9], [31] or partial scribble labels [5], [29]. Due to the limited structure information in the weak annotations, the performance of existing weakly supervised models is still far from satisfactory, and the main focus of existing weakly supervised salient object detection

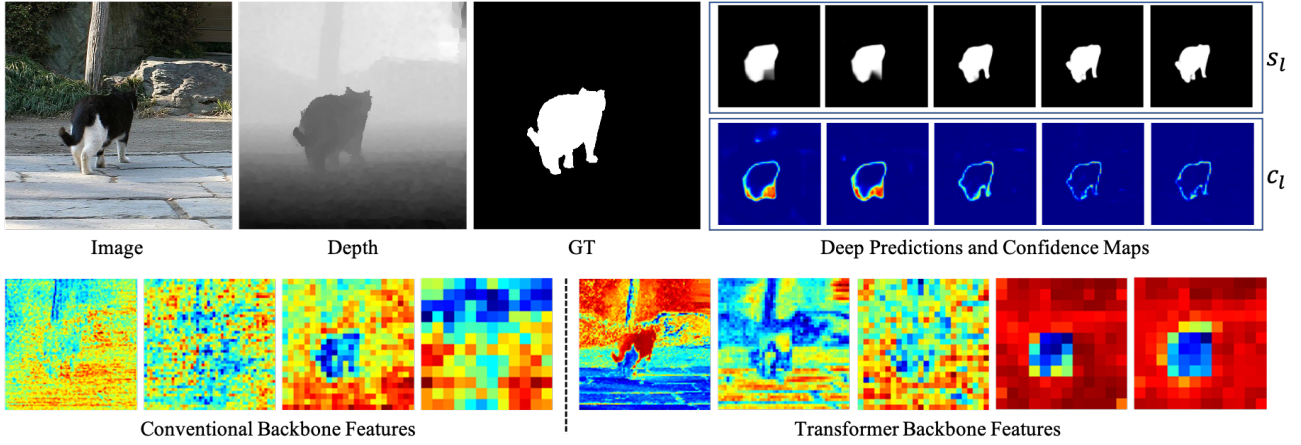


Fig. 3. Results from our difficulty-aware RGB-D SOD network via a deeply supervised transformer and visualizations of the feature maps compared with a conventional convolution backbone.

models is to recover the structure information by designing the pair-wise constraints related regularizer.

**RGB-D Image Pair based Fully Supervised Salient Object Detection:** As there exists the depth data in the RGB-D image pair, one of the main focuses of the fully supervised RGB-D image pair based salient object detection models is to explore the complementary information between the RGB image and the depth data. Depending on how information from these two modalities is fused, existing RGB-D salient object detection models can be divided into three categories: early-fusion models [3], [32], late-fusion models [33], [34], [35] and cross-level fusion models [4], [36], [37], [38], [39], [40], [41], [42], [43], [44], [45], [46], [47]. The early-fusion models fuse RGB image and depth data in the input layer, forming a four-channel feature map. The late fusion models treat each mode (RGB and depth) separately, and then saliency fusion is achieved at the output layer. The cross-level fusion models gradually fuse feature of RGB and depth [4], [41], [42], [44], [46], [47], [48], [49], [50].

**Camouflaged Object Detection:** Camouflaged object detection is an important biological phenomenon that animals attempt to hide into the surroundings and thus deceive the viewers [51]. In early studies, the camouflaged object detection is defined as contrast based task, where the contrast computed by the handcrafted features, such as edges, brightness, corner points and texture to separate the camouflaged object and the background [52], [53], [54], [55], [56]. However, the manual features are vulnerable to the attack from the sophisticated camouflage strategies. Therefore, the recent research turns to the deep learning to incorporate more structure information about the object for detection. Le *et al.* [57] proposes to employ an auxiliary classification network to discriminate the images containing the camouflaged objects and segment the objects through the segmentation network. Fan *et al.* [58] constructs SINet that composed of a search module to search the candidate regions and an identification module for precise localization. Ren *et al.* [59] formulates texture-aware refinement modules and emphasizing the difference between the texture-aware features. Dong *et al.* [60] uses a significant large receptive field to provide rich context information and an effective fusion strategy to aggregate features with different levels of representation.

**Transformer Network and its Application:** Transformer [22] is a set-to-set method based on self-attention mechanism, which achieved great success in natural language processing (NLP). The

breakthroughs from Transformer networks in NLP domain has sparked great interest in the computer vision community to adapt these models for vision tasks such as object detection [61], [62], [63], [64], [65], image segmentation [23], [64], [66], object tracking [67], [68], [69], pose estimation [70], [71], optical flow [72] *etc.*. The dense prediction tasks aim to perform pixel-level classification or regression on the feature map. In recent years, dense prediction tasks usually usefully convolutional neural networks (FCNs), which adopt convolution and sub-sampling with different feature attention or enhancement methods as their fundamental elements in order to learn multi-scale representations. Inspired by the success of Vision Transformer (ViT) [73] in the task of image classification, some works extend such classification model as a backbone for dense prediction tasks. SETR [66] directly feeds the sequence of image vectors to a standard Transformer encoder, and the decoder is simple several convolutional layers which upsamples feature maps to origin size. PVT [64] is based on the design of ViT, while also maintaining the global receptive field. This method introduces a progressive shrinking pyramid to reduce the sequence length of the transformer when the network depth increases, thereby significantly reducing the amount of calculation. DPT [23] uses a U-shape structure, which uses ViT as encoder to encode features from different spatial resolutions of the initial embedding throughout all transformer stages. And a decoder assembles the set of tokens into image-like feature representations at various resolutions. Such feature representations are progressively fused into the final dense prediction. Liu *et al.* [24] present the Swin Transformer, a hierarchical transformer with a shifted windowing scheme to achieve an efficient network for vision tasks.

### 3 OUR METHOD

#### 3.1 Transformer Network: An Overview

**Multi-Head Self Attention:** The typical idea in transformer networks is self-attention, which captures long-term dependencies between elements in an input sequence. The self-attention mechanism aims to estimate the relevance of one item to other items in a given sequence, which explicitly models the interactions between all items of a sequence.

We denote a sequence  $X \in \mathbb{R}^{n \times d}$ , where  $n$  is the sequence length and  $d$  is the embedding dimension as input vector. The input vector is first transformed into three different vectors: the

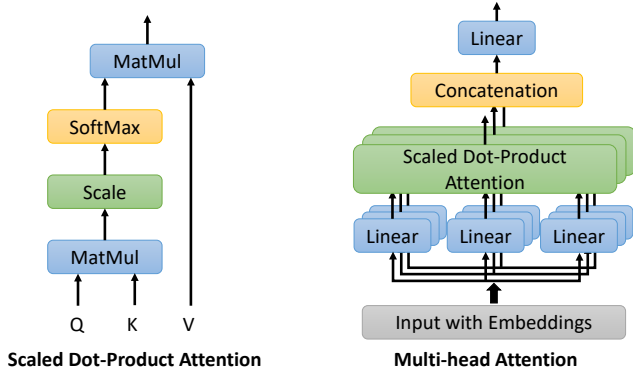


Fig. 4. “Multi-Head Attention” consists of several “Scaled Dot-Product Attention” layers running in parallel.

query vector  $Q$ , the key vector  $K$  and the value vector  $V$  with the same dimension  $d$ . This is done by defining three learnable weight matrices  $W^Q \in \mathbb{R}^{n \times d_q}$ ,  $W^K \in \mathbb{R}^{n \times d_k}$  and  $W^V \in \mathbb{R}^{n \times d_v}$ . The input sequence  $X$  is projected onto these weight matrices to get:

$$Q = XW^Q, K = XW^K, V = XW^V. \quad (1)$$

Based on the above three weight matrices, we compute the dot-product of the query with all keys. Then the results are normalized into attention scores using the softmax operator. Finally, each value vector is multiplied by the sum of the attention scores. In this way, vectors with larger attention scores receive additional focus from the following layers. The definition of scaled dot-product self-attention is:

$$Z = \text{softmax}\left(\frac{QK^T}{\sqrt{d}}\right)V. \quad (2)$$

The output of the self-attention layer is independent of the input order. To solve the missing positional information of input vectors, an additional positional encoding is added to the inputs. There are two optional encoding forms, including learnable parameters and sine/cosine functions encoding. The form of the latter is as follows:

$$\begin{aligned} PE(pos, 2i) &= \sin\left(\frac{pos}{10000^{\frac{2i}{d}}}\right), \\ PE(pos, 2i+1) &= \cos\left(\frac{pos}{10000^{\frac{2i}{d}}}\right), \end{aligned} \quad (3)$$

where  $pos$  is the position of the word in a vector and  $i$  is the dimension of the positional encoding, thus each dimension of the positional encoding corresponds to a sinusoid.

The self-attention is then extended to multi-head self-attention to perform the self-attention layer in parallel. Specifically, as shown in Fig. 4, to project the inputs into different representations, different weight matrices are used for different heads. Features then pass through the multi-head attention layer, and are concatenated to get the final results by another linear projection.

**Transformer Network:** In Fig. 5, the vanilla Transformer [22] is composed of a multi-layer encoder module and a multi-layer decoder module, which was firstly applied on the machine translation task in neural language processing (NLP). Each encoder is composed of a multi-head self attention layer and a feed-forward network, while each decoder is composed of a multi-head self attention layer, an encoder-decoder attention layer and a feed-forward network [74].

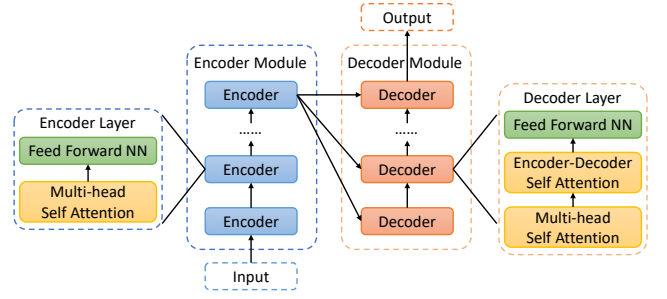


Fig. 5. The structure of vanilla Transformer.

### 3.2 Vision Transformer Network

Vision transformer is designed for dense prediction tasks, *e.g.* semantic segmentation or depth estimation [23], [24]. For a typical vision transformer, the input image  $x \in \mathbb{R}^{H \times W \times C}$  is split into a sequence of patches (or tokens)  $x = [x_1, \dots, x_N] \in \mathbb{R}^{N \times P^2 \times C}$  with patch size  $(P, P)$ , where  $C$  is channel of image  $x$ . Then each token is linearly projected to a sequence of one dimensional patch embedding feature vectors as  $e_x = [E x_1, \dots, E x_N] \in \mathbb{R}^{N \times d}$ , where  $E$  is the embedding function,  $d$  is the dimension of the feature space. As no position information is encoded in  $e_x$ , the learnable position embeddings  $pos$  are then added to the sequence as  $z = e_x + pos$  in order to capture the spatial location information.

With the tokenization of input image  $x$ , all the tokens  $z$  are fed into a transformer encoder with  $L$  transformer layers. Each transformer layer includes a multi-head self-attention (MSA) module and a feed forward multilayer perceptron (MLP) block with layer normalization LN. The  $i$ -th,  $i \in \{1, \dots, L\}$  transformer layer can be expressed as:

$$\begin{aligned} a^{i-1} &= \text{MSA}(\text{LN}(z^{i-1})) + z^{i-1}; \\ z^i &= \text{MLP}(\text{LN}(a^{i-1})) + a^{i-1}, i = 1, \dots, L. \end{aligned} \quad (4)$$

The state at the output of the transformer encoder ( $z^L$ ) then serves as the image representation.

The core components of (4) is MSA, which allows the model to attend to information from different representation subspaces at different positions [22]. To compute self-attention, the input vector is first transformed into three different vectors: query  $Q$ , key  $K$  and value  $V$  of the same dimension  $d$  by three linear layers. Then the definition of self-attention is defined as  $Z = \text{softmax}(QK^T/\sqrt{d})V$ .

### 3.3 Transformer based Salient Object Detection

We argue that the local-connection attributes of CNNs makes them less effective for exploring accurate global context information for SOD. Then we introduce a unified transformer backbone [24] based salient object detection network to achieve effective context modeling as shown in Fig. 6. Two main modules are included in our unified framework, namely the saliency “Generator” to produce saliency predictions with deep supervision, and the confidence estimation based “Discriminator” to estimate pixel-wise confidence map and achieve difficulty-aware learning.

#### 3.3.1 Generator

The saliency “Generator” is composed of the “Transformer Encoder” module  $E_\theta(x)$  and the “Deep Supervision” module







Fig. 8. Scribble annotations label part of foreground/background region, where the yellow scribble indicates the salient foreground, and blue scribble shows the background region.

structural similarity index measure [79] and  $L_1$  loss, which is defined as:

$$\mathcal{L}_{ss}^l = \alpha * SSIM(s_l^s, s_l^\alpha) + (1 - \alpha) * L_1(s_l^s, s_l^\alpha), l = 1, \dots, 5, \quad (7)$$

where  $s_l^s = G_\beta(E_\theta(x^\alpha))$ , which is the output of the generator with the re-scaled image  $x^\alpha$  as input, and we set the scale rate as  $\alpha = 0.85$  in our experiments. Accordingly,  $s_l^\alpha$  is re-scaled model prediction with the original image  $x$  as input. Further, given the scribble annotation, we adopt the partial cross-entropy loss  $\mathcal{L}_{pce}^l$  to constrain predictions on the scribble region. In this way, we define the loss function for the weakly-supervised model as:

$$\mathcal{L}_{weak}^l = \mathcal{L}_{pce}^l + \lambda_1 * \mathcal{L}_{sm}^l + \lambda_2 * \mathcal{L}_{grcf}^l + \lambda_3 * \mathcal{L}_{ss}^l, l = 1, \dots, 5. \quad (8)$$

Empirically, we set the loss weights as  $\lambda_1 = \lambda_2 = 0.3$  and  $\lambda_3 = 1$ . The final weakly-supervised loss function is then defined as:  $\mathcal{L}_{weak} = Ave(\{\mathcal{L}_{weak}^l\}_{l=1}^5)$ .

### 3.3.2 Discriminator

The discriminator  $R_\gamma$  is composed of five convolutional layers of kernel size 3, which takes the concatenation of image  $x$  and the model predictions  $s_l$  as input, and produces one channel confidence map  $c_l$ .  $\gamma$  is parameter set of the discriminator. We define supervision of the discriminator as the difference between model prediction and the ground truth saliency map as:  $g_l = |y - s_l|$ . Note that, for the weakly-supervised setting, we define the supervision for the discriminator as  $g_l = |y - mask(s_l)|$ , where  $mask$  is a binary mask with the scribble foreground and background as 1 and other area as 0. In this way, the discriminator is designed to recognize the difference of prediction and ground truth. We define the loss function for the discriminator as binary cross-entropy loss  $\mathcal{L}_{dis} = Ave(\{\mathcal{L}_{ce}(sigmoid(R_\gamma(s_l, x)), g_l)\}_{l=1}^5)$ , where  $sigmoid$  is the sigmoid function.

**Difficulty-aware learning:** The goal of difficulty-aware learning is similar to hard negative mining [80] that aims to emphasize more on the hard samples. With the proposed discriminator, our model can estimate pixel-wise accuracy of its prediction as shown in Fig. 3, which serves as a good indicator of pixel-wise difficulty of samples, as the model produces more accurate predictions for easy samples than for hard samples. Given predictions  $s_l$  from the generator and output from the discriminator  $c_l = sigmoid(R_\gamma(s_l, x))$ , we replace the edge-aware weight  $\omega$  in Eq. 5 and Eq. 6 with  $c_l$ , and define it as the difficulty-aware loss  $\mathcal{L}_d^l$ . Then the difficulty-aware loss for multiple predictions is defined as  $\mathcal{L}_d = Ave(\{\mathcal{L}_d^l\}_{l=1}^5)$ . With  $\mathcal{L}_d$  and the fully-supervised loss,  $\mathcal{L}_{full}^g$ , we obtain the final loss function for the fully-supervised learning models as:  $\mathcal{L}_{full} = 0.5 * (\mathcal{L}_{full}^g + \mathcal{L}_d)$ . As the estimated difficulty map (shown in Fig. 12 “Ours\_W”) is less accurate due to the sparse scribble annotation, we only apply difficulty-aware learning for the two fully-supervised models, and “Discriminator” in the weakly-supervised model only serve as confidence estimation module.

## 4 EXPERIMENTAL RESULTS

### 4.1 Task Introduction

For static image based salient object detection, we perform experiments on RGB salient object detection, RGB-D salient object detection and weakly supervised RGB salient object detection, which covers both fully supervised saliency segmentation and weakly supervised saliency segmentation. For camouflaged object detection, we only conduct experiments on fully supervised RGB image based camouflaged object detection.

### 4.2 Setup

**Dataset:** For the salient object detection task, we train the models by using DUTS training dataset [6], and test on six other widely used data sets: the DUTS testing dataset, ECSSD [81], DUT [11], HKU-IS [82], PASCAL-S [83] and the SOD testing dataset [84]. For weakly supervised RGB image based salient object detection, we train our model using the DUTS-S training dataset [5] with scribble annotations, and testing on above six benchmark RGB saliency testing dataset. For the camouflaged object detection task, we train the models using the COD10K training dataset [58], and test them on four test datasets: CAMO [57], CHAMELEON [89], the COD10K testing dataset, and NC4K [90]. For RGB-D salient object detection models, we follow the conventional training setting, in which the training set is a combination of 1,485 images from the NJU2K dataset [91] and 700 images from the NLPR dataset [92]. We then test the performance of our model and competing models on the NJU2K testing set, NLPR testing set LFSD [93], DES [94], SSB [95] and the SIP [96] testing set.

**Evaluation Metrics:** For all the four tasks, we use four evaluation indicators to measure the performance, including Mean Absolute Error  $\mathcal{M}$ , Mean F-measure ( $F_\beta$ ), Mean E-measure ( $E_\xi$ ) [97] and S-measure ( $S_\alpha$ ) [98].

**MAE**  $\mathcal{M}$  is defined as the pixel-wise difference between the predicted  $c$  and the pixel-wise binary ground-truth  $y$ :

$$MAE = \frac{1}{H \times W} |c - y|, \quad (9)$$

where  $H$  and  $W$  are the height and width of  $c$  correspondingly.

**F-measure**  $F_\beta$  is a region based similarity metric, and we provide the mean F-measure using varying fixed (0-255) thresholds.

**E-measure**  $E_\xi$  is the recent proposed Enhanced alignment measure [97] in the binary map evaluation field to jointly capture image-level statistics and local pixel matching information.

**S-measure**  $S_\alpha$  is a structure based measure [98], which combines the region-aware ( $S_r$ ) and object-aware ( $S_o$ ) structural similarity as their final structure metric:

$$S_\alpha = \alpha S_o + (1 - \alpha) S_r, \quad (10)$$

where  $\alpha \in [0, 1]$  is the balance parameter and set to 0.5 as default.

**Implementation Details:** We train our model in Pytorch with the Swin transformer backbone [24] trained on ImageNet-1K [99], and other newly added layers are randomly initialized. We resize all the images and ground truth to  $384 \times 384$ . The maximum epoch is 50. The initial learning rates are  $2.5 \times 10^{-5}$  for all the three tasks. The whole training takes 13 hours, 20 hours, 3 hours and 6 hours with batch size 6 on one NVIDIA GTX 2080Ti GPUs for fully-supervised RGB SOD, weakly-supervised RGB SOD, RGB-D image pair based SOD and RGB image based COD respectively.

TABLE 1  
Performance comparison with benchmark RGB SOD models.

Method	DUTS [6]				ECSSD [81]				DUT [11]				HKU-IS [82]				PASCAL-S [83]				SOD [84]			
	$S_\alpha \uparrow$	$F_\beta \uparrow$	$E_\xi \uparrow$	$M \downarrow$	$S_\alpha \uparrow$	$F_\beta \uparrow$	$E_\xi \uparrow$	$M \downarrow$	$S_\alpha \uparrow$	$F_\beta \uparrow$	$E_\xi \uparrow$	$M \downarrow$	$S_\alpha \uparrow$	$F_\beta \uparrow$	$E_\xi \uparrow$	$M \downarrow$	$S_\alpha \uparrow$	$F_\beta \uparrow$	$E_\xi \uparrow$	$M \downarrow$	$S_\alpha \uparrow$	$F_\beta \uparrow$	$E_\xi \uparrow$	$M \downarrow$
Fully-supervised SOD Models																								
CPD [17]	.869	.821	.898	.043	.913	.909	.937	.040	.825	.742	.847	.056	.906	.892	.938	.034	.848	.819	.882	.071	.799	.779	.811	.088
SCRN [1]	.885	.833	.900	.040	.920	.910	.933	.041	.837	.749	.847	.056	.916	.894	.935	.034	.869	.833	.892	.063	.817	.790	.829	.087
PoolNet [85]	.887	.840	.910	.037	.919	.913	.938	.038	.831	.748	.848	.054	.919	.903	.945	.030	.865	.835	.896	.065	.820	.804	.834	.084
BASNet [86]	.876	.823	.896	.048	.910	.913	.938	.040	.836	.767	.865	.057	.909	.903	.943	.032	.838	.818	.879	.076	.798	.792	.827	.094
EGNet [87]	.878	.824	.898	.043	.914	.906	.933	.043	.840	.755	.855	.054	.917	.900	.943	.031	.852	.823	.881	.074	.824	.811	.843	.081
F3Net [2]	.888	.852	.920	.035	.919	.921	.943	.036	.839	.766	.864	.053	.917	.910	.952	.028	.861	.835	.898	.062	.824	.814	.850	.077
ITSD [88]	.886	.841	.917	.039	.920	.916	.943	.037	.842	.767	.867	.056	.921	.906	.950	.030	.860	.830	.894	.066	.836	.829	.867	.076
Ours_F	<b>.909</b>	<b>.877</b>	<b>.945</b>	<b>.028</b>	<b>.935</b>	<b>.934</b>	<b>.961</b>	<b>.026</b>	<b>.860</b>	<b>.799</b>	<b>.891</b>	<b>.050</b>	<b>.932</b>	<b>.924</b>	<b>.966</b>	<b>.023</b>	<b>.879</b>	<b>.856</b>	<b>.916</b>	<b>.052</b>	<b>.863</b>	<b>.862</b>	<b>.899</b>	<b>.063</b>
Weakly-supervised SOD Models																								
SSAL [5]	.803	.747	.865	.062	.863	.865	.908	.061	.785	.702	.835	.068	.865	.858	.923	.047	.798	.773	.854	.093	.750	.743	.801	.108
WSS [6]	.748	.633	.806	.100	.808	.774	.801	.106	.730	.590	.729	.110	.822	.773	.819	.079	.701	.691	.687	.187	.698	.635	.687	.152
C2S [30]	.805	.718	.845	.071	-	-	-	-	.773	.665	.810	.082	.869	.837	.910	.053	.784	.806	.813	.130	.770	.741	.799	.117
SCWS [29]	.841	.818	.901	.049	.879	.894	.924	.051	.813	.751	.856	.060	.883	.892	.938	.038	.821	.815	.877	.078	.782	.791	.833	.090
Ours_W	<b>.860</b>	<b>.823</b>	<b>.915</b>	<b>.040</b>	<b>.906</b>	<b>.913</b>	<b>.951</b>	<b>.038</b>	<b>.838</b>	<b>.768</b>	<b>.888</b>	<b>.056</b>	<b>.899</b>	<b>.893</b>	<b>.954</b>	<b>.034</b>	<b>.848</b>	<b>.823</b>	<b>.902</b>	<b>.065</b>	<b>.817</b>	<b>.818</b>	<b>.872</b>	<b>.080</b>

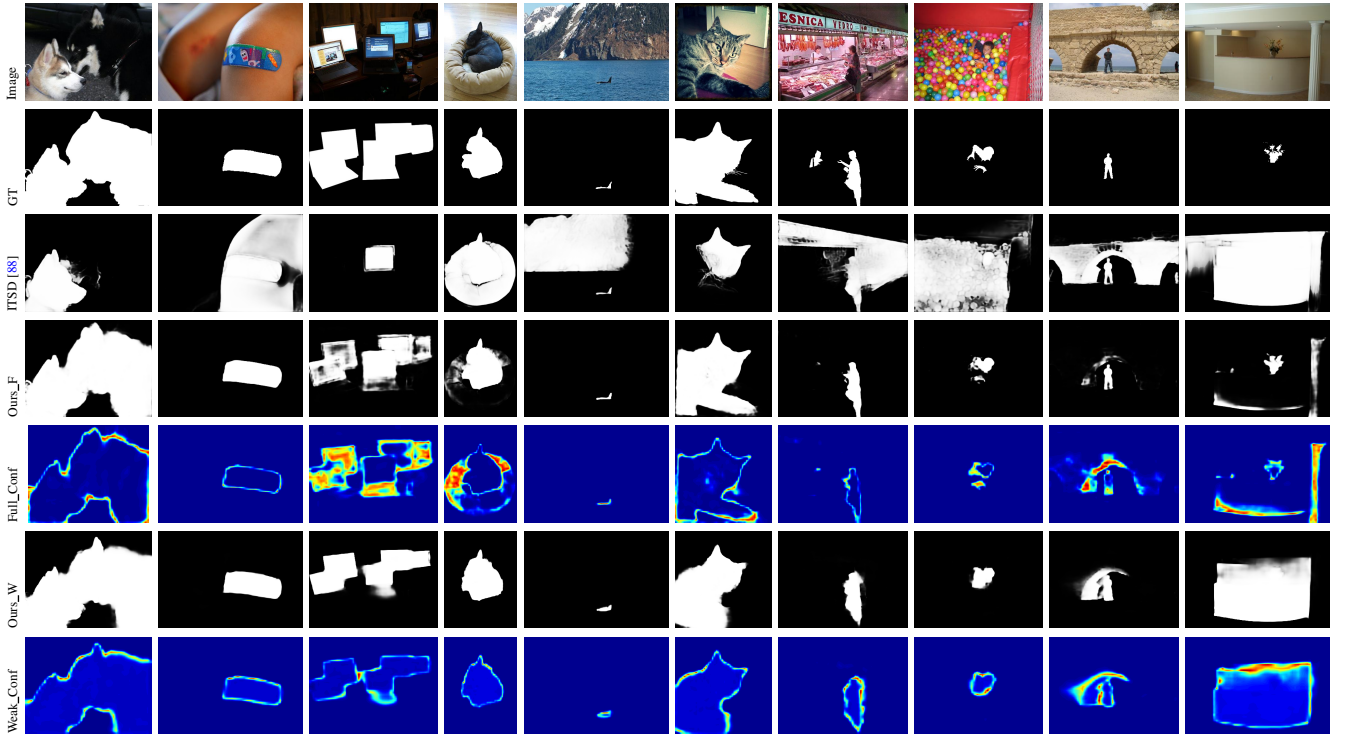


Fig. 9. Predictions of SOTA RGB SOD model (ITSD [88]) and our transformer backbone based models.

### 4.3 RGB image based models

#### 4.3.1 Saliency/Camouflage Detection

As a context based task, the existing salient object detection models aim to identify and segment image parts that attract human visual attention. Specifically, the SOD models focus on effectively aggregating features of different stages of the backbone network to achieve fine-grained predictions. However, when the salient target is more complex, the existing conventional backbone based SOD models fail to segment the complete object as shown in Fig. 9. With the capability of long-range dependency modeling, the transformer backbone [24] can model effective global context information, leading to better performance as shown in Fig. 9 “Ours\_F” and Table 1 “Ours\_F”. Fig. 9 shows that with the superior context modeling ability, our model is effective in detecting

both large salient objects (1<sup>st</sup> and 6<sup>th</sup> column) and small salient objects (5<sup>th</sup> and 8<sup>th</sup> column), leading to scale-robust model.

Similar to SOD, COD is also a contrast based task. However, the foreground of COD dataset usually has low contrast compared with its surrounding, as the prey evolves to have similar pattern as its surrounding to avoid being recognized by predators. The goal of camouflaged object detection model is to identify and segment objects that are camouflaged in the environment. The existing camouflaged object detection techniques [58], [90], [101] design camouflaged object detection networks with convolutional neural network following a similar pipeline as salient object detection, which usually involves an encoder to extract camouflage features, and a decoder to aggregate features from different levels of network to produce an one channel camouflage map. Due to

TABLE 2  
Performance comparison with benchmark camouflaged object detection models.

Method	CAMO [57]				CHAMELEON [89]				COD10K [58]				NC4K [90]			
	$S_\alpha \uparrow$	$F_\beta \uparrow$	$E_\xi \uparrow$	$\mathcal{M} \downarrow$	$S_\alpha \uparrow$	$F_\beta \uparrow$	$E_\xi \uparrow$	$\mathcal{M} \downarrow$	$S_\alpha \uparrow$	$F_\beta \uparrow$	$E_\xi \uparrow$	$\mathcal{M} \downarrow$	$S_\alpha \uparrow$	$F_\beta \uparrow$	$E_\xi \uparrow$	$\mathcal{M} \downarrow$
SCRN [1]	.779	.705	.796	.090	.876	.787	.889	.042	.789	.651	.817	.047	.832	.759	.855	.059
CSNet [100]	.771	.705	.795	.092	.856	.766	.869	.047	.778	.635	.810	.047	.819	.748	.845	.061
EGNet [87]	.735	.650	.753	.102	.856	.763	.877	.049	.748	.587	.776	.053	.796	.718	.830	.067
LSR [90]	.793	.725	.826	.085	.893	.839	.938	.033	.793	.685	.868	.041	.839	.779	.883	.053
UJSC [101]	.803	.759	.853	.076	.894	.848	.943	.030	.817	.726	.892	.035	.842	.806	.898	.047
MGL [102]	.775	.726	.812	.088	.893	.834	.918	.030	.814	.711	.852	.035	.833	.782	.867	.052
PFNet [103]	.782	.744	.840	.085	.882	.826	.922	.033	.800	.700	.875	.040	.829	.782	.886	.053
PraNet [104]	.769	.711	.825	.094	.860	.790	.908	.044	.790	.672	.861	.045	.822	.763	.877	.059
SINet [58]	.745	.702	.804	.092	.872	.827	.936	.034	.776	.679	.864	.043	.810	.772	.873	.057
SINet-V2 [105]	.820	.782	.882	.070	.888	.835	.942	.030	.815	.718	.887	.037	.847	.805	.903	.048
Ours	<b>.860</b>	<b>.832</b>	<b>.920</b>	<b>.050</b>	<b>.899</b>	<b>.858</b>	<b>.958</b>	<b>.023</b>	<b>.843</b>	<b>.765</b>	<b>.917</b>	<b>.029</b>	<b>.872</b>	<b>.837</b>	<b>.927</b>	<b>.037</b>

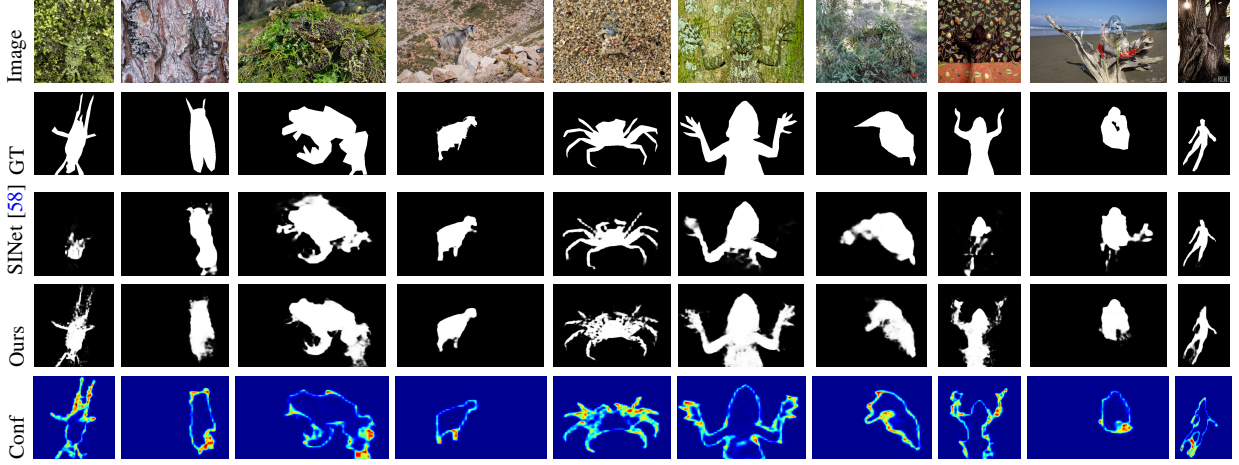


Fig. 10. Predictions of the state-of-the-art camouflaged object detection model (SINet [58]) and our transformer backbone based model.

TABLE 3  
Performance comparison with benchmark RGB-D SOD models.

Method	NJU2K [91]				SSB [95]				DES [94]				NLPR [92]				LFSD [93]				SIP [96]			
	$S_\alpha \uparrow$	$F_\beta \uparrow$	$E_\xi \uparrow$	$\mathcal{M} \downarrow$	$S_\alpha \uparrow$	$F_\beta \uparrow$	$E_\xi \uparrow$	$\mathcal{M} \downarrow$	$S_\alpha \uparrow$	$F_\beta \uparrow$	$E_\xi \uparrow$	$\mathcal{M} \downarrow$	$S_\alpha \uparrow$	$F_\beta \uparrow$	$E_\xi \uparrow$	$\mathcal{M} \downarrow$	$S_\alpha \uparrow$	$F_\beta \uparrow$	$E_\xi \uparrow$	$\mathcal{M} \downarrow$	$S_\alpha \uparrow$	$F_\beta \uparrow$	$E_\xi \uparrow$	$\mathcal{M} \downarrow$
BBSNet [4]	.921	.902	.938	.035	.908	.883	.928	.041	.933	.910	.949	.021	.930	.896	.950	.023	.864	.843	.883	.072	.879	.868	.906	.055
BiaNet [45]	.915	.903	.934	.039	.904	.879	.926	.043	.931	.910	.948	.021	.925	.894	.948	.024	.845	.834	.871	.085	.883	.873	.913	.052
CoNet [43]	.911	.903	.944	.036	.896	.877	.939	.040	.906	.880	.939	.026	.900	.859	.937	.030	.842	.834	.886	.077	.868	.855	.915	.054
UCNet [3]	.897	.886	.930	.043	.903	.884	.938	.039	.934	.919	.967	.019	.920	.891	.951	.025	.864	.855	.901	.066	.875	.867	.914	.051
JLDCF [106]	.902	.885	.935	.041	.903	.873	.936	.040	.931	.907	.959	.021	.925	.894	.955	.022	.862	.848	.894	.070	.880	.873	.918	.049
Ours	<b>.928</b>	<b>.919</b>	<b>.955</b>	<b>.028</b>	<b>.915</b>	<b>.894</b>	<b>.947</b>	<b>.034</b>	<b>.942</b>	<b>.931</b>	<b>.971</b>	<b>.015</b>	<b>.932</b>	<b>.913</b>	<b>.962</b>	<b>.020</b>	<b>.877</b>	<b>.864</b>	<b>.904</b>	<b>.062</b>	<b>.897</b>	<b>.897</b>	<b>.933</b>	<b>.041</b>

the smaller receptive field of those models, the existing techniques fail to identify camouflaged objects when they share too similar pattern to their surroundings as shown in Fig. 10 “SINet [58]”. Our transformer backbone based camouflaged object detection network “Ours” in Table 2 achieve better performance compared with those recent models. The results shown in Fig. 10 “Ours” further shows that our model achieves consistent better performance for various scales of camouflaged objects, illustrating again the scale-robustness property of transformer backbone based models.

#### 4.3.2 Weakly-supervised Salient Object Detection

Following [5], [29], we design a transformer backbone [23] based weakly supervised salient object detection model to learn saliency from scribble annotations, and the performance is shown in Table 1 “Ours\_W”, which shows a consistent better performance of the proposed framework. Although the weak model achieves inferior

performance than our fully-supervised model, we can still observe nearly accurate prediction with reasonable object boundaries as shown in Fig. 9 “Ours\_W”.

#### 4.3.3 Confidence Estimation

In Fig. 9 and Fig. 10, we also show model predictions from the proposed discriminator, where “Full\_Conf”, “Weak\_Conf” are the normalized discriminator predictions  $\text{sigmoid}(R_\gamma(s_1, x))$ . “COD\_Conf” is the confidence maps for the camouflaged object detection model. We observe meaningful discriminator outputs for the fully-supervised models, which can indeed highlight the less accurate regions. However, the output of discriminator for the weakly-supervised model cannot always accurately localize the incorrect predictions ( $3^{rd}$  and last column), making it less effective for difficulty-aware learning, and we are working on fixing this issue.



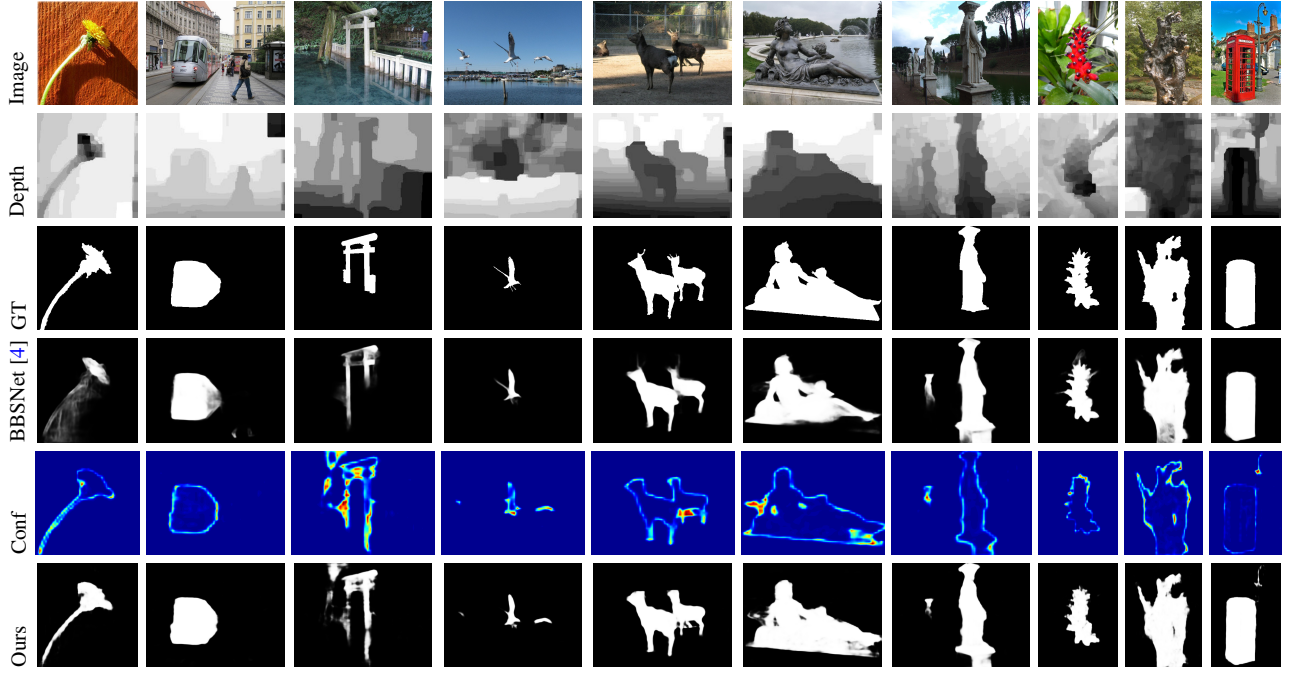


Fig. 11. Predictions of the state-of-the-art RGB-D salient object detection model (BBSNet [4]) and our transformer based model.

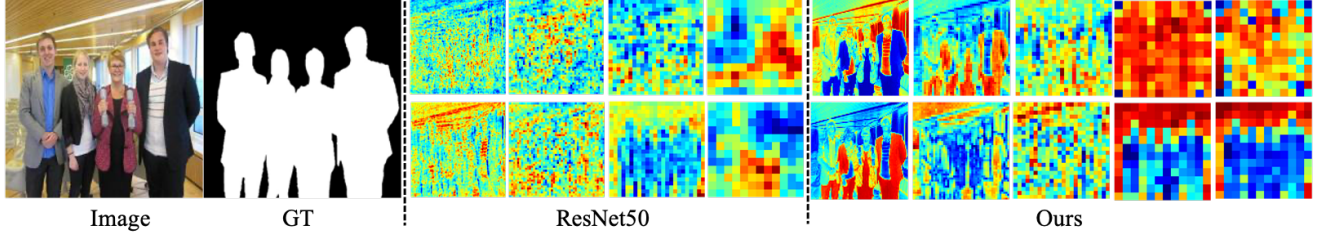


Fig. 12. Different levels of features for the ResNet50 backbone [16] and our transformer backbone before ( $1^{st}$  row of each image) and after fine-tune them for SOD ( $2^{nd}$  row of each image).

#### 4.4 RGB-D based Models

For RGB-D based models, we only investigate RGB-D salient object detection, and design a similar network as the RGB salient object detection model, except that we concatenate RGB image and depth data in the input layer and feed it to a  $3 \times 3$  convolutional layer to obtain a feature map of channel size 3, which is then fed to the “Transformer Encoder” in Fig. 6. The performance of our transformer backbone based RGB-D salient object detection model is shown in Table 3, which clearly verifies the effectiveness of our solution. We also show failure cases of the state-of-the-art models and our corresponding predictions (and the confidence maps “RGBD\_Conf”) in Fig. 11, which further demonstrate the superiority of our network, which is effective in achieving multi-scale salient object detection.

#### 4.5 Running-time Comparison:

Our framework has a total parameters number of 89M, which is similar to existing models, *e.g.*, BASNet [86] and JLDCF [106] have 87M and 144M parameters respectively. For inference, our model achieve 46fps, which is comparable with existing models.

#### 4.6 Feature Visualization:

We prove effectiveness of the transformer backbone for SOD and COD in Table 1, Table 3 and Table 2. According to existing

analysis [23], [24], [73], this mainly comes from the powerful long-range dependency estimation, leading to effective context information modeling. To achieve better understanding of the transformer network, we analyze different levels of features of the conventional backbone (*e.g.*, ResNet50 [16]) and our transformer backbone [24] before ( $1^{st}$  row) and after ( $2^{nd}$  row) fine-tuning them for SOD as shown in Fig. 12<sup>2</sup>. The backbone features (from left to right) in Fig. 12 indicate lower to higher level features. We observe that: **1)** the lower level features change less before and after fine-tuning the backbone models for SOD; **2)** the lower level features of transformer backbone shows better structure information than ResNet50 backbone [16]; **3)** after fine-tuning for SOD, higher level features of the transformer backbone include more accurate semantic information. With this observation, we conclude that the transformer backbone encodes more accurate object structure information and more distinct semantic information.

#### 4.7 Model Analysis

In this section, we analyse our transformer backbone based models in detail. Note that, all the following experiments are based on the

<sup>2</sup> We averaged feature map of each level ( $t_l$  from our backbone) channel-wise, and then perform min-max normalization to generate the feature for visualization.

TABLE 4  
Model analysis related experiments.

Method	DUTS [6]				ECSSD [81]				DUT [11]				HKU-IS [82]				PASCAL-S [83]				SOD [84]			
	$S_\alpha \uparrow$	$F_\beta \uparrow$	$E_\xi \uparrow$	$\mathcal{M} \downarrow$	$S_\alpha \uparrow$	$F_\beta \uparrow$	$E_\xi \uparrow$	$\mathcal{M} \downarrow$	$S_\alpha \uparrow$	$F_\beta \uparrow$	$E_\xi \uparrow$	$\mathcal{M} \downarrow$	$S_\alpha \uparrow$	$F_\beta \uparrow$	$E_\xi \uparrow$	$\mathcal{M} \downarrow$	$S_\alpha \uparrow$	$F_\beta \uparrow$	$E_\xi \uparrow$	$\mathcal{M} \downarrow$	$S_\alpha \uparrow$	$F_\beta \uparrow$	$E_\xi \uparrow$	$\mathcal{M} \downarrow$
Conventional backbone																								
ResNet50	.879	.844	.919	.037	.922	.924	.952	.033	.827	.756	.863	.055	.913	.909	.953	.029	.857	.850	.903	.065	.828	.826	.862	.074
ResNet50_SGD	.873	.838	.913	.038	.917	.918	.948	.035	.816	.750	.859	.056	.914	.910	.950	.030	.849	.845	.900	.067	.825	.820	.859	.075
ResNet50_R	.757	.668	.817	.090	.831	.823	.876	.082	.755	.652	.807	.088	.833	.809	.895	.065	.743	.721	.794	.131	.715	.697	.769	.138
Other Transformer as Backbone																								
Base_DPT	.916	.888	.948	.026	.937	.938	.962	.026	.868	.812	.898	.049	.937	.930	.969	.021	.881	.858	.916	.052	.864	.864	.901	.061
DPT	.921	.897	.954	.023	.935	.937	.959	.027	.869	.813	.901	.046	.937	.931	.970	.020	.887	.869	.925	.048	.867	.870	.903	.059
Deep supervision and difficulty-aware learning analysis																								
Base	.898	.859	.940	.031	.927	.923	.955	.031	.852	.783	.888	.052	.920	.905	.958	.029	.874	.850	.914	.055	.845	.836	.885	.068
Base_DS	.903	.870	.941	.029	.933	.932	.959	.028	.854	.796	.888	.051	.930	.917	.960	.025	.870	.851	.910	.053	.854	.854	.887	.065
Base_DA	.904	.876	.940	.028	.933	.932	.958	.027	.858	.794	.889	.051	.930	.923	.963	.024	.873	.854	.913	.053	.855	.849	.886	.066
Ours_R	.782	.688	.820	.089	.859	.836	.888	.074	.769	.661	.801	.097	.853	.817	.894	.063	.772	.719	.803	.124	.740	.705	.777	.137
Ours_SGD	.890	.856	.916	.036	.923	.914	.948	.034	.846	.769	.872	.053	.920	.908	.957	.030	.861	.836	.905	.067	.833	.841	.871	.075
Ours_F	.909	.877	.945	.028	.935	.934	.961	.026	.860	.799	.891	.050	.932	.924	.966	.023	.879	.856	.916	.052	.863	.862	.899	.063
Ours_22k	.919	.893	.953	.025	.936	.937	.961	.026	.870	.815	.901	.045	.937	.931	.969	.021	.888	.871	.926	.047	.863	.865	.901	.060

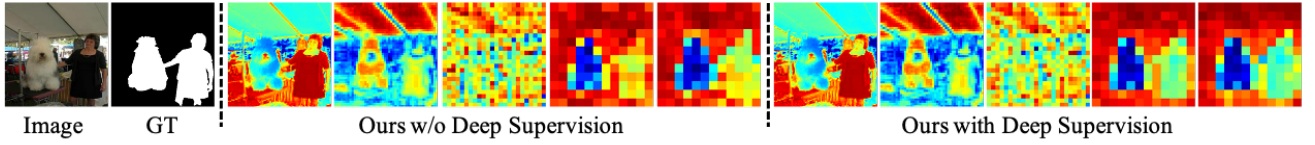


Fig. 13. Features of using and without using the deep supervision strategy.

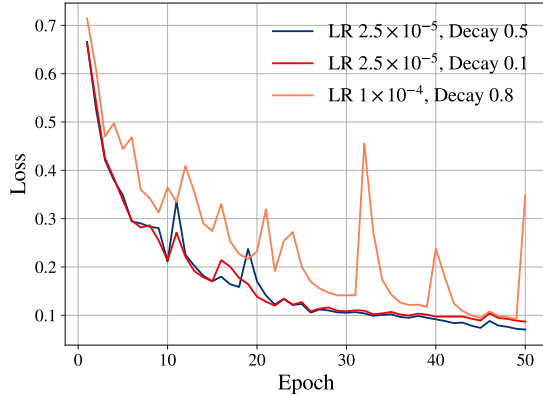


Fig. 14. Loss convergence curves of our transformer backbone based salient object detection network.

fully supervised RGB salient object detection task. We highlight the result in **blue** if it's better than our final result.

**Model performance w.r.t. learning rate and optimizer:** We observe the transformer backbone based network is sensitive to the initial learning rate. We then analyse the loss convergence of the transformer backbone based network as shown in Fig. 14, which clearly shows that a larger learning rate may lead to significant instability in training. Further, we want to analyse how conventional backbone and transformer backbone perform with different optimizers. We change our backbone network to ResNet50 [16], and obtain model performance as shown in Table 4 “ResNet50”, which uses Adam as optimizer. Then, we train the model with SGD as optimizer, which is “ResNet50\_SGD”. We observe that for the conventional backbone based network, e.g., ResNet50, the SGD optimizer (“ResNet50\_SGD”) and Adam optimizer (“ResNet50”) achieve similar performance. However, for the transformer backbone based network, the Adam optimizer

(“Ours\_F”) achieves significantly better performance than the model with SGD optimizer (“Ours\_SGD”). We will investigate it further in the future.

**The importance of initialization weights:** Note that, for both conventional backbone and our transformer backbone, we initialize them with the image classification model trained on ImageNet-1K [99]. To test how the initialization weights contribute to model performance, we randomly initialize the two models (“ResNet50” and “Ours\_F” in Table 4) and obtain model performance as “ResNet50\_R” and “Ours\_R” in Table 4. We observe worse performance of both “ResNet50\_R” and “Ours\_R”, which further illustrates the necessity of fine-tuning the backbone models for SOD. We also initialize our transformer backbone with parameters pre-trained on ImageNet-22K dataset, and show the result as “Ours\_22k” in Table 4. The better performance of “Ours\_22k” compared with “Ours\_F” further explains importance of the initialization weights for the backbone network.

**The contribution of deep supervision and difficulty-aware learning:** We claim that the global context information in each level of the transformer backbone, as well as the necessity of accurate spatial information modeling makes it both suitable and desirable to perform deep supervision at every level of the network. Further, inspired by hard negative mining [80], we argue difficulty-aware learning can be beneficial for SOD. To test how the deep supervision and difficulty-aware learning contribute to our framework, we remove the two modules from our pipeline, and define prediction of this base model as  $s = D_m[d_1, \dots, d_5]$ , where  $D_m$  is the DenseASPP module [76]. Note that we upsample  $\{d_i\}_{i=2}^5$  to the same spatial size of  $d_1$  before concatenation. The performance of this base model is shown as “Base” in Table 4. Then we add the deep supervision and difficulty-aware learning module to “Base” and obtain “Base\_DS” and “Base\_DA” respectively. The improved performance of “Base\_DS” and “Base\_DA” indicates effectiveness of each strategy. Further, we visualize back-

TABLE 5  
Weakly supervised learning rated loss analysis.

Method	DUTS [6]				ECSSD [81]				DUT [11]				HKU-IS [82]				PASCAL-S [83]				SOD [84]			
	$S_\alpha \uparrow$	$F_\beta \uparrow$	$E_\xi \uparrow$	$\mathcal{M} \downarrow$	$S_\alpha \uparrow$	$F_\beta \uparrow$	$E_\xi \uparrow$	$\mathcal{M} \downarrow$	$S_\alpha \uparrow$	$F_\beta \uparrow$	$E_\xi \uparrow$	$\mathcal{M} \downarrow$	$S_\alpha \uparrow$	$F_\beta \uparrow$	$E_\xi \uparrow$	$\mathcal{M} \downarrow$	$S_\alpha \uparrow$	$F_\beta \uparrow$	$E_\xi \uparrow$	$\mathcal{M} \downarrow$	$S_\alpha \uparrow$	$F_\beta \uparrow$	$E_\xi \uparrow$	$\mathcal{M} \downarrow$
Base	.770	.660	.820	.074	.846	.799	.891	.070	.745	.617	.783	.092	.821	.754	.876	.071	.786	.720	.832	.096	.765	.717	.822	.107
SSI	.780	.673	.830	.071	.852	.803	.896	.067	.758	.634	.795	.088	.833	.767	.885	.066	.797	.732	.841	.091	.779	.732	.839	.098
Smooth	.818	.752	.884	.058	.874	.863	.927	.052	.798	.712	.844	.072	.863	.836	.926	.049	.822	.789	.881	.078	.789	.774	.859	.090
GCRF	.801	.712	.856	.060	.873	.846	.922	.051	.775	.668	.816	.078	.857	.813	.915	.050	.816	.770	.867	.079	.786	.752	.845	.094
Ours_W	<b>.860</b>	<b>.823</b>	<b>.915</b>	<b>.040</b>	<b>.906</b>	<b>.913</b>	<b>.951</b>	<b>.038</b>	<b>.838</b>	<b>.768</b>	<b>.888</b>	<b>.056</b>	<b>.899</b>	<b>.883</b>	<b>.954</b>	<b>.034</b>	<b>.848</b>	<b>.823</b>	<b>.902</b>	<b>.065</b>	<b>.817</b>	<b>.818</b>	<b>.872</b>	<b>.080</b>

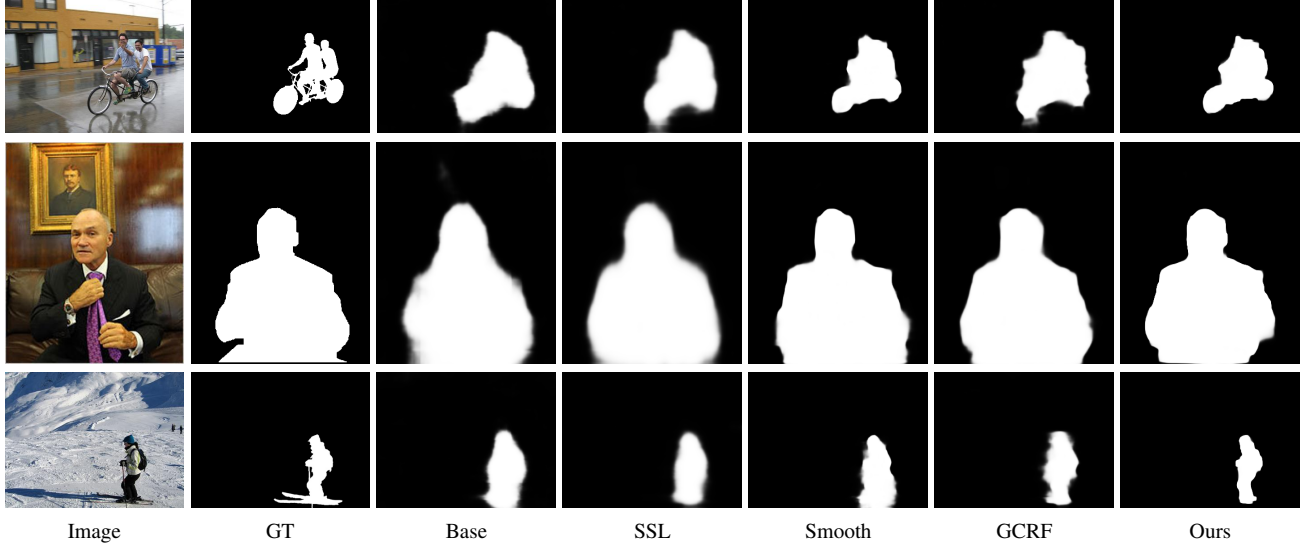


Fig. 15. Model predictions of different weakly supervised related loss functions.

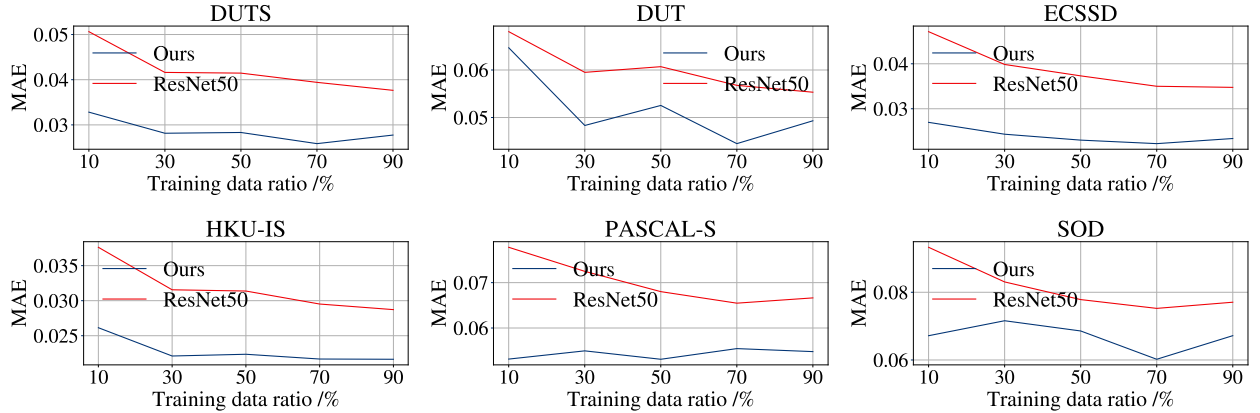


Fig. 16. Model performance of ResNet50 [16] backbone and our transformer backbone based salient object detection network w.r.t. different training dataset sizes on six testing dataset.

bone features of model without deep supervision (“Base\_DA”) and our model with deep supervision in Fig. 13 and find a clear difference between the two backbone features is the degree of the higher level semantic information encoding. We argue that the deep supervision can be beneficial for the higher level features to achieve uniform activation within the same semantic object.

**Different transformer backbone analysis:** Following our pipeline, we change the Swin transformer backbone [24] to DPT backbone [23], and achieve “Base\_DPT” and “DPT” in Table 4 respectively, where “Base\_DPT” has the same network structure as “Base” in Table 4 except that we change the backbone to DPT

[23], and “DPT” have all our proposed components, *e.g.* deep supervision and difficulty-aware learning. Note that, the DPT backbone we used in Table 4 is initialized with weights trained on ImageNet-22K. The better performance of “DPT” compared with “Base\_DPT” illustrates the effectiveness of the two strategies. Although the DPT backbone [23] based model (“DPT”) outperforms the Swin backbone [24] based model (“Ours\_F”), our model with Swin backbone initialized with ImageNet-22K (“Ours\_22k”) achieve comparable performance as “DPT”, which further explains the necessity of initial weights for the backbones.

**Weakly-supervised loss analysis:** Beside the partial cross-

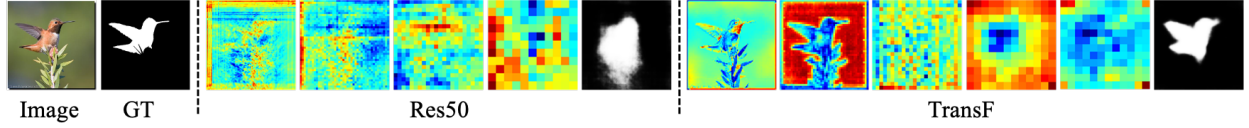


Fig. 17. Features of ResNet50 backbone and the transformer backbone for weakly-supervised SOD.

TABLE 6  
Performance of different backbone models for weakly-supervised SOD.

Method	DUTS [6]				ECSSD [81]				DUT [11]				HKU-IS [82]				PASCAL-S [83]				SOD [84]			
	$S_\alpha \uparrow$	$F_\beta \uparrow$	$E_\xi \uparrow$	$\mathcal{M} \downarrow$	$S_\alpha \uparrow$	$F_\beta \uparrow$	$E_\xi \uparrow$	$\mathcal{M} \downarrow$	$S_\alpha \uparrow$	$F_\beta \uparrow$	$E_\xi \uparrow$	$\mathcal{M} \downarrow$	$S_\alpha \uparrow$	$F_\beta \uparrow$	$E_\xi \uparrow$	$\mathcal{M} \downarrow$	$S_\alpha \uparrow$	$F_\beta \uparrow$	$E_\xi \uparrow$	$\mathcal{M} \downarrow$	$S_\alpha \uparrow$	$F_\beta \uparrow$	$E_\xi \uparrow$	$\mathcal{M} \downarrow$
Res50	.599	.456	.622	.202	.692	.601	.720	.185	.606	.429	.621	.203	.664	.546	.706	.182	.645	.544	.669	.213	.623	.527	.666	.218
TransF	.770	.660	.820	.074	.846	.799	.891	.070	.745	.617	.783	.092	.821	.754	.876	.071	.786	.720	.832	.096	.765	.717	.822	.107
Ours_W	<b>.860</b>	<b>.823</b>	<b>.915</b>	<b>.040</b>	<b>.906</b>	<b>.913</b>	<b>.951</b>	<b>.038</b>	<b>.838</b>	<b>.768</b>	<b>.888</b>	<b>.056</b>	<b>.899</b>	<b>.883</b>	<b>.954</b>	<b>.034</b>	<b>.848</b>	<b>.823</b>	<b>.902</b>	<b>.065</b>	<b>.817</b>	<b>.818</b>	<b>.872</b>	<b>.080</b>

TABLE 7  
Self-supervised learning verification.

Method	DUTS [6]				ECSSD [81]				DUT [11]				HKU-IS [82]				PASCAL-S [83]				SOD [84]			
	$S_\alpha \uparrow$	$F_\beta \uparrow$	$E_\xi \uparrow$	$\mathcal{M} \downarrow$	$S_\alpha \uparrow$	$F_\beta \uparrow$	$E_\xi \uparrow$	$\mathcal{M} \downarrow$	$S_\alpha \uparrow$	$F_\beta \uparrow$	$E_\xi \uparrow$	$\mathcal{M} \downarrow$	$S_\alpha \uparrow$	$F_\beta \uparrow$	$E_\xi \uparrow$	$\mathcal{M} \downarrow$	$S_\alpha \uparrow$	$F_\beta \uparrow$	$E_\xi \uparrow$	$\mathcal{M} \downarrow$	$S_\alpha \uparrow$	$F_\beta \uparrow$	$E_\xi \uparrow$	$\mathcal{M} \downarrow$
Scale	.908	.877	.944	.028	.934	<b>.935</b>	.960	.027	.859	.797	.890	.050	<b>.933</b>	<b>.925</b>	.966	<b>.022</b>	.879	<b>.859</b>	<b>.918</b>	.052	.860	.857	.895	<b>.060</b>
Rotation	<b>.911</b>	<b>.884</b>	<b>.947</b>	<b>.027</b>	.933	<b>.935</b>	.959	.027	<b>.863</b>	<b>.806</b>	<b>.898</b>	<b>.047</b>	.932	<b>.925</b>	.966	.023	<b>.881</b>	<b>.864</b>	<b>.921</b>	<b>.050</b>	.857	.858	.891	.065
Ours_F	<b>.909</b>	<b>.877</b>	<b>.945</b>	<b>.028</b>	<b>.935</b>	<b>.934</b>	<b>.961</b>	<b>.026</b>	<b>.860</b>	<b>.799</b>	<b>.891</b>	<b>.050</b>	<b>.932</b>	<b>.924</b>	<b>.966</b>	<b>.023</b>	<b>.879</b>	<b>.856</b>	<b>.916</b>	<b>.052</b>	<b>.863</b>	<b>.862</b>	<b>.899</b>	<b>.063</b>

entropy loss, we use three extra loss functions for weakly-supervised salient object detection, namely smoothness loss to constrain the predictions to be well aligned with the image edges, gated CRF loss to regularize the pairwise term predictions which aims to produce similar predictions for spatially similar pixels, and a self-supervised loss to effectively learn from fewer supervision with consistency loss, *e.g.* scale-invariant predictions. We then carried out extra experiments to verify the effectiveness of each loss function, and show the results in Table 5. Note that, all the experiments in this section are built upon the base model in our main paper Table 3. “Base” is the base performance with only the partial cross-entropy loss. “SSI”, “Smooth” and “GCRF” are models of adding self-supervised loss, smoothness loss and gated CRF loss to the “Base” respectively. We observe improved performance of each extra loss function, which explains the effectiveness of them. Further, we find that the smoothness and gated CRF achieve more performance gain than the self-supervised loss, which mainly comes from the effective structure modeling of each of the two loss functions. We also show predictions of each model in Fig. 15. It’s clear that both the base model with only partial cross-entropy loss (“Base”) and the model with extra self-supervised loss (“SSL”) fail to accurately localize object boundaries, leading to blurred predictions. The smoothness loss and the gated CRF loss work better in modeling the structure information, leading to more accurate predictions, especially along object edges.

#### 4.8 Discussion

**Model performance with different numbers of training datasets:** We train our transformer backbone networks and ResNet50 [16] backbone network in Table 4 with different numbers of training datasets, which are 10%, 30%, 50%, 70%, 90% of the entire training dataset respectively, and show model performance in Fig. 16. The consistently better performance of the transformer backbone based model with regard to different numbers of training example explains the effectiveness of our

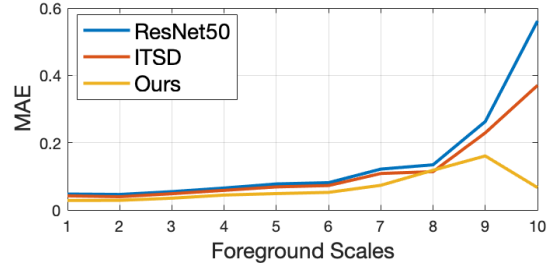


Fig. 18. Model performance (MAE) w.r.t. scales of salient objects.

solution. Further, we observe that the model performance is not always increasing with a larger training dataset, which inspires us to work on active learning based transformer network to actively select representative samples for model training.

**Transformer backbone VS CNN backbone for weakly-supervised SOD:** We observe clear object structure in the transformer backbone within the lower level features as shown in Fig. 12. We then design two different models with ResNet50 [16] and Swin transformer [24] as backbone. The decoder part is the same as “Base” in Table 4. We train the two models with only partial cross-entropy loss, and we show their corresponding results in Table 6 “Res50” and “TransF” respectively. The significantly better performance of “TransF” compared with “Res50” shows the effectiveness of the transformer backbone for weakly-supervised salient object detection. We also visualize the feature of the two trained models in Fig. 17, where heat maps are the features and binary maps are the predictions. We observe clear structure information in “TranF”, which explains the superior performance of the transformer for weakly-supervised learning via supervisions with less structure information [107].

**Self-supervised learning and Transformer:** Self-supervised learning is proven effective [108] within the transformer network for image classification. We then carry out experiments with



TABLE 8  
Fusion strategy analysis

Method	NJU2K [91]				SSB [95]				DES [94]				NLPR [92]				LFSD [93]				SIP [96]			
	$S_\alpha \uparrow$	$F_\beta \uparrow$	$E_\xi \uparrow$	$\mathcal{M} \downarrow$	$S_\alpha \uparrow$	$F_\beta \uparrow$	$E_\xi \uparrow$	$\mathcal{M} \downarrow$	$S_\alpha \uparrow$	$F_\beta \uparrow$	$E_\xi \uparrow$	$\mathcal{M} \downarrow$	$S_\alpha \uparrow$	$F_\beta \uparrow$	$E_\xi \uparrow$	$\mathcal{M} \downarrow$	$S_\alpha \uparrow$	$F_\beta \uparrow$	$E_\xi \uparrow$	$\mathcal{M} \downarrow$	$S_\alpha \uparrow$	$F_\beta \uparrow$	$E_\xi \uparrow$	$\mathcal{M} \downarrow$
Cross	.930	.921	.955	.028	.912	.888	.946	.034	.935	.924	.964	.017	.934	.915	.963	.020	.878	.868	.904	.062	.904	.903	.938	.038
Late	.928	.921	.955	.028	.914	.891	.947	.033	.924	.912	.952	.020	.936	.916	.965	.019	.881	.872	.908	.060	.900	.904	.935	.040
Ours	.928	.919	.955	.028	.915	.894	.947	.034	.942	.931	.971	.015	.932	.913	.962	.020	.877	.864	.904	.062	.897	.897	.933	.041

TABLE 9  
Difficulty-aware learning analysis.

Method	DUTS [6]				ECSSD [81]				DUT [11]				HKU-IS [82]				PASCAL-S [83]				SOD [84]			
	$S_\alpha \uparrow$	$F_\beta \uparrow$	$E_\xi \uparrow$	$\mathcal{M} \downarrow$	$S_\alpha \uparrow$	$F_\beta \uparrow$	$E_\xi \uparrow$	$\mathcal{M} \downarrow$	$S_\alpha \uparrow$	$F_\beta \uparrow$	$E_\xi \uparrow$	$\mathcal{M} \downarrow$	$S_\alpha \uparrow$	$F_\beta \uparrow$	$E_\xi \uparrow$	$\mathcal{M} \downarrow$	$S_\alpha \uparrow$	$F_\beta \uparrow$	$E_\xi \uparrow$	$\mathcal{M} \downarrow$	$S_\alpha \uparrow$	$F_\beta \uparrow$	$E_\xi \uparrow$	$\mathcal{M} \downarrow$
Ours_F	.909	.877	.945	.028	.935	.934	.961	.026	.860	.799	.891	.050	.932	.924	.966	.023	.879	.856	.916	.052	.863	.862	.899	.063
DA1	.910	.880	.946	.028	.935	.935	.960	.027	.863	.804	.896	.048	.932	.925	.966	.023	.881	.861	.918	.051	.862	.862	.898	.062
DA2	.909	.879	.945	.029	.935	.935	.961	.026	.860	.800	.892	.049	.933	.925	.966	.023	.881	.859	.920	.052	.863	.861	.900	.061

TABLE 10  
Performance of the weakly-supervised SOD model with auxiliary edge detection module.

Method	DUTS [6]				ECSSD [81]				DUT [11]				HKU-IS [82]				PASCAL-S [83]				SOD [84]			
	$S_\alpha \uparrow$	$F_\beta \uparrow$	$E_\xi \uparrow$	$\mathcal{M} \downarrow$	$S_\alpha \uparrow$	$F_\beta \uparrow$	$E_\xi \uparrow$	$\mathcal{M} \downarrow$	$S_\alpha \uparrow$	$F_\beta \uparrow$	$E_\xi \uparrow$	$\mathcal{M} \downarrow$	$S_\alpha \uparrow$	$F_\beta \uparrow$	$E_\xi \uparrow$	$\mathcal{M} \downarrow$	$S_\alpha \uparrow$	$F_\beta \uparrow$	$E_\xi \uparrow$	$\mathcal{M} \downarrow$	$S_\alpha \uparrow$	$F_\beta \uparrow$	$E_\xi \uparrow$	$\mathcal{M} \downarrow$
Ours_W	.860	.823	.915	.040	.906	.913	.951	.038	.838	.768	.888	.056	.899	.883	.954	.034	.848	.823	.902	.065	.817	.818	.872	.080
Ours_E	.865	.817	.922	.040	.910	.907	.951	.035	.831	.755	.873	.058	.905	.891	.954	.031	.850	.826	.901	.065	.823	.818	.880	.075

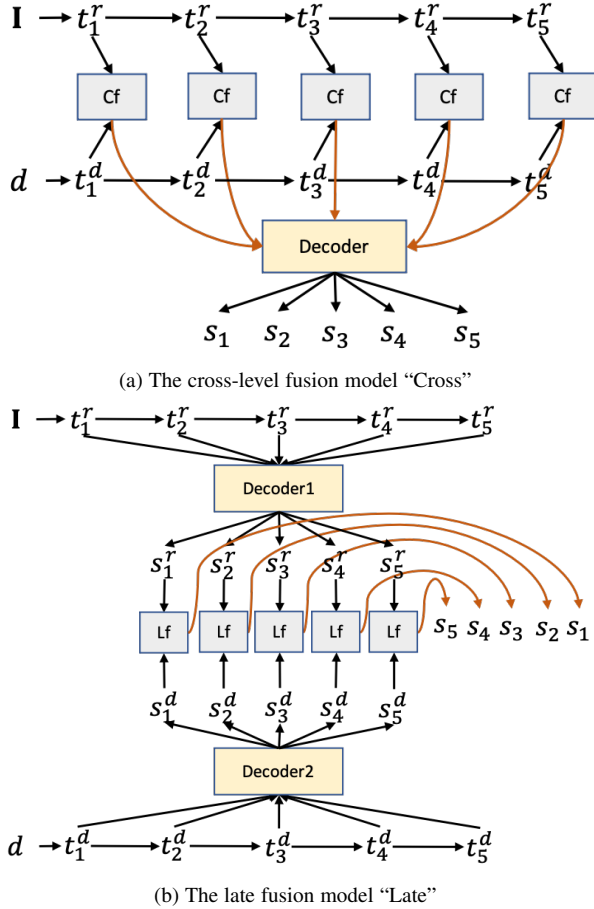


Fig. 19. Detailed pipeline of the two extra RGB-D fusion models, where "Cf" module is the cascaded concatenation operation, residual channel attention module [75] and the  $3 \times 3$  convolutional layers with batch normalization to obtain fused feature map of channel size  $C = 32$ , and "Lf" is the cascaded concatenation operation and  $3 \times 3$  convolutional layers with batch normalization to produce the saliency map.

two widely used self-supervised learning strategy, *e.g.*, scale and rotation transformation with cycle consistency loss (as in Eq. 7). The results are reported in Table 7 as "Scale" and "Rotation" respectively. We observe comparable or worse performance with additional self-supervised learning, indicating self-supervised learning may be less effective in our scenario due to the high capacity of the transformer encoder.

**Training data size and salient object scales:** Both size of the training dataset and scales of salient objects play an important role for conventional backbone based SOD. We analyze our model performance (MAE) on four testing dataset w.r.t. training dataset size (x-axis of Fig. 16 represents the percentage of the DUTS training dataset [6] we used) and scale of salient objects (10 times the x-axis of Fig. 18 is the percentage of the salient foreground) and find: 1) the transformer backbone is more robust to size of training dataset as shown in Fig. 16, which makes it suitable to learn from smaller training dataset; 2) the conventional backbone based models (ITSD [88]) perform worse for images with large salient objects, while the transformer backbone can perform well on this scenario, leading to scale-robust model.

**RGB-D salient object detection model analysis:** To achieve a unified salient object detection network, we design an early fusion RGB-D salient object detection network. To test how the model performs with different fusion strategies, we design two extra frameworks with both cross level fusion and late fusion models as shown in Fig. 19 (a) and (b), where "Decoder", "Decoder1" and "Decoder2" have the same decoder structure as in Fig. 7. The results are shown in Table 8 "Cross" and "Late" respectively. Note that, the models are designed with our whole network structure, including both deep supervision and difficulty-aware learning. We observe similar performance of each fusion strategies, which clearly shows that early-fusion model can achieve comparable performance with other two fusion models.

**Difficulty-aware learning analysis** In the difficulty-aware learning part, we define the supervision for the discriminator as  $g_l = |y - s_l|$ . To test how the supervision of the discriminator af-

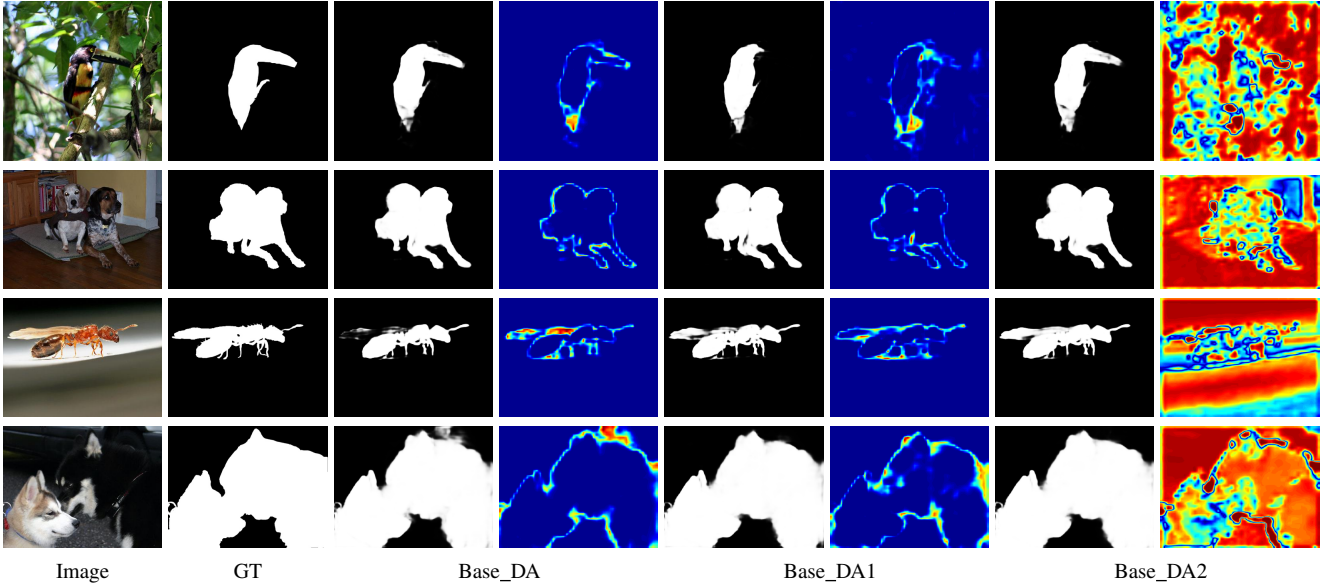


Fig. 20. Predictions and the confidence maps of different difficulty-aware learning strategies.

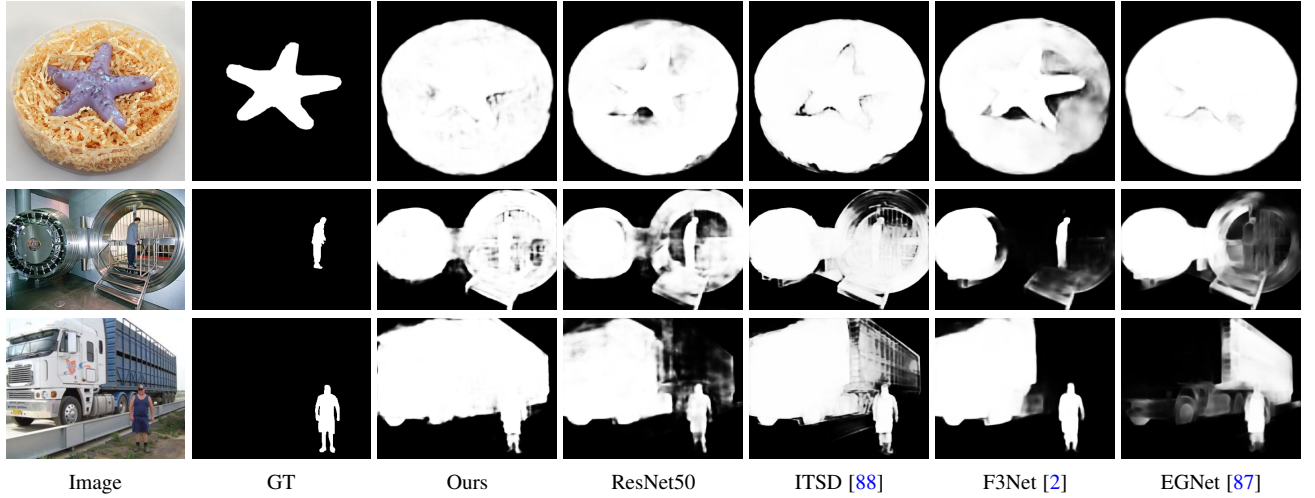


Fig. 21. Failed cases of our model compared with existing techniques.

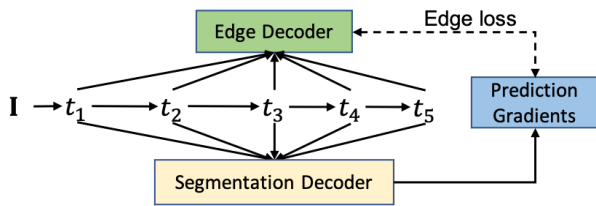


Fig. 22. Auxiliary edge detection module for weakly-supervised SOD.

fect model performance, we define  $g_l^1 = y*(1-s_l) + (1-y)*s_l$  to achieve difficulty-aware learning similar to [109], and  $g_l^2 = \{0, 1\}$  to achieve adversarial learning [110]. For the latter, we define supervision of the discriminator with prediction as input as **0** matrix and with ground truth saliency map as input as **1** matrix. The performance of each model is shown as “Base\_DA1” and “Base\_DA2” respectively for  $g_l^1$  and  $g_l^2$ . Note that, those models are built up the base framework without deep supervision as shown

in the main paper Table 3 “Base”.

We observe similar performance of our model “Base\_DA” compared with “Base\_DA1” with  $g_l^1$  as supervision, while relative worse performance with  $g_l^2$  as supervision. This indicates that it’s more effective to have a supervision of the discriminator that can reflect the pixel-wise awareness of accuracy. We also show the output confidence map from each model in Fig. As the output of “Base\_DA2” aims to distinguish predictions and ground truth saliency map, which leads to a **0.5** matrix, indicating the discriminator cannot distinguish prediction and ground truth. We then define confidence map for “Base\_DA2” as  $|\text{sigmoid}(R_\gamma(s_l, x)) - 0.5|$ , where  $R_\gamma$  is the discriminator, and  $s_l$  is the prediction. Fig. 20 shows that the confidence maps from both our “Base\_DA” and “Base\_DA1” can reflect the pixel-wise awareness of model prediction, while “Base\_DA2” fails to do so.

**Auxiliary edge detection module for weakly-supervised SOD:** As discussed in [5], [111], the auxiliary edge detection module can be beneficial for weakly-supervised segmentation within the convolutional neural network framework. We then analyse how

the edge detection module contributes to weakly-supervised SOD within the transformer framework. To achieve this, we design an edge detection module following [112] as shown in Fig. 22, which include an extra “Edge Decoder” to generate salient edge maps same as [112]. The “Segmentation Decoder” is same as “Decoder” in Fig. 19 (a), and the “Prediction Gradients” module computes the gradients magnitude of the finest level prediction ( $s_1$  in this paper). The auxiliary edge detection module introduce extra loss function, namely the “Edge loss”, which is defined as binary cross-entropy loss between the estimated edge map from the “Edge Decoder” and the edge map of the model prediction. The final loss function of model in Fig. 22 includes our original weakly supervised loss  $\mathcal{L}_{weak}$  and the extra edge loss. We show performance of this model in Table 10 “Ours\_E”. The observe slightly better performance of “Ours\_E”, which explains contribution of the auxiliary edge detection module for weakly-supervised SOD. The parameter number of “Ours\_E” is 90M, which is relatively larger than “Ours\_W”, which is 89M.

**Failure case analysis:** We analyse when our transformer backbone based model fails, and show some samples in Fig. 21, where “ResNet50” is the ResNet50 model for salient object detection in Table 4. We observe the main less accurate predictions are those with too much false positive. This can be caused by at least two reasons. Firstly, the generated binary ground truth might be biased, which focus mostly on person (images in the 2<sup>nd</sup>, 3<sup>rd</sup>, 4<sup>th</sup> rows). Secondly, the subtle contrast difference for the foreground regions is difficult to be perceived by the deep model (image in the 1<sup>st</sup> row), which makes salient object ranking [113] an interesting direction to work on. We will work on solving the above two problems in the future.

## 5 CONCLUSION

In this paper, we study the context information learning problem under the transformer backbone for salient object detection (SOD). Specifically, we design a unified framework for fully-supervised RGB image based SOD, RGB-D image pair based SOD and weakly-supervised RGB image based SOD. We observe that the accurate structure information encoded in the transformer backbone as shown in Fig. 12 makes it powerful for weakly-supervised SOD. Further, we investigate deep supervision and difficulty-aware learning within the transformer backbone. The former is demonstrated to restore the gradients from lower level features to higher level features, thus enabling uniform activation within the same semantic object, and the latter is effective in identifying the hard pixels for effective hard negative mining. We also analyze features within the CNN backbone and transformer backbone and find that the more accurate structure information and distinct semantic information within the lower and higher level feature respectively differentiate the two sets of backbone models. As an extension, we train a camouflaged object detection network with our fully supervised model, and observe consistent improve performance. Extensive experimental results demonstrate the superiority of our transformer backbone based network, achieving new benchmarks for the three different SOD tasks and one COD task, which also inspires us to extend our framework to other related tasks [114], [115].

## REFERENCES

[1] Z. Wu, L. Su, and Q. Huang, “Stacked cross refinement network for edge-aware salient object detection,” in *Proceedings of the IEEE*

*International Conference on Computer Vision (ICCV)*, pp. 7264–7273, 2019.

[2] J. Wei, S. Wang, and Q. Huang, “F<sup>3</sup>net: Fusion, feedback and focus for salient object detection,” in *Proceedings of the AAAI Conference on Artificial Intelligence (AAAI)*, pp. 12321–12328, 2020.

[3] J. Zhang, D.-P. Fan, Y. Dai, S. Anwar, F. S. Saleh, T. Zhang, and N. Barnes, “UC-Net: Uncertainty inspired RGB-D saliency detection via conditional variational autoencoders,” in *Proceedings of the IEEE Conference on Computer Vision and Pattern Recognition (CVPR)*, pp. 8582–8591, 2020.

[4] D.-P. Fan, Y. Zhai, A. Borji, J. Yang, and L. Shao, “BBS-Net: RGB-D salient object detection with a bifurcated backbone strategy network,” in *Proceedings of the European Conference on Computer Vision (ECCV)*, pp. 275–292, 2020.

[5] J. Zhang, X. Yu, A. Li, P. Song, B. Liu, and Y. Dai, “Weakly-supervised salient object detection via scribble annotations,” in *Proceedings of the IEEE Conference on Computer Vision and Pattern Recognition (CVPR)*, pp. 12546–12555, 2020.

[6] L. Wang, H. Lu, Y. Wang, M. Feng, D. Wang, B. Yin, and X. Ruan, “Learning to detect salient objects with image-level supervision,” in *Proceedings of the IEEE Conference on Computer Vision and Pattern Recognition (CVPR)*, pp. 136–145, 2017.

[7] W. Wang, Q. Lai, H. Fu, J. Shen, H. Ling, and R. Yang, “Salient object detection in the deep learning era: An in-depth survey,” *IEEE Transactions on Pattern Analysis and Machine Intelligence (T-PAMI)*, pp. 1–1, 2021.

[8] J. Zhang, T. Zhang, Y. Dai, M. Harandi, and R. Hartley, “Deep unsupervised saliency detection: A multiple noisy labeling perspective,” in *Proceedings of the IEEE Conference on Computer Vision and Pattern Recognition (CVPR)*, pp. 9029–9038, 2018.

[9] D. T. Nguyen, M. Dax, C. K. Mummadi, T. P. N. Ngo, T. H. P. Nguyen, Z. Lou, and T. Brox, “DeepUSPS: Deep robust unsupervised saliency prediction with self-supervision,” in *Proceedings of the Advances in Neural Information Processing Systems (NeurIPS)*, 2019.

[10] W. Zhu, S. Liang, Y. Wei, and J. Sun, “Saliency optimization from robust background detection,” in *Proceedings of the IEEE Conference on Computer Vision and Pattern Recognition (CVPR)*, pp. 2814–2821, 2014.

[11] C. Yang, L. Zhang, H. Lu, X. Ruan, and M.-H. Yang, “Saliency detection via graph-based manifold ranking,” in *Proceedings of the IEEE Conference on Computer Vision and Pattern Recognition (CVPR)*, pp. 3166–3173, 2013.

[12] M.-M. Cheng, N. J. Mitra, X. Huang, P. H. Torr, and S.-M. Hu, “Global contrast based salient region detection,” *IEEE Transactions on Pattern Analysis and Machine Intelligence (T-PAMI)*, vol. 37, no. 3, pp. 569–582, 2014.

[13] Z. Luo, A. Mishra, A. Achkar, J. Eichel, S. Li, and P.-M. Jodoin, “Non-local deep features for salient object detection,” in *Proceedings of the IEEE Conference on Computer Vision and Pattern Recognition (CVPR)*, pp. 6609–6617, 2017.

[14] N. Liu, J. Han, and M.-H. Yang, “Picanet: Learning pixel-wise contextual attention for saliency detection,” in *Proceedings of the IEEE Conference on Computer Vision and Pattern Recognition (CVPR)*, pp. 3089–3098, 2018.

[15] K. Simonyan and A. Zisserman, “Very deep convolutional networks for large-scale image recognition,” in *Proceedings of the The International Conference on Learning Representations (ICLR)* (Y. Bengio and Y. LeCun, eds.), 2015.

[16] K. He, X. Zhang, S. Ren, and J. Sun, “Deep residual learning for image recognition,” in *Proceedings of the IEEE Conference on Computer Vision and Pattern Recognition (CVPR)*, pp. 770–778, 2016.

[17] Z. Wu, L. Su, and Q. Huang, “Cascaded partial decoder for fast and accurate salient object detection,” in *Proceedings of the IEEE Conference on Computer Vision and Pattern Recognition (CVPR)*, pp. 3907–3916, 2019.

[18] L. Itti, C. Koch, and E. Niebur, “A model of saliency-based visual attention for rapid scene analysis,” *IEEE Transactions on Pattern Analysis and Machine Intelligence (T-PAMI)*, vol. 20, no. 11, pp. 1254–1259, 1998.

[19] R. Achanta, S. Hemami, F. Estrada, and S. Susstrunk, “Frequency-tuned salient region detection,” in *Proceedings of the IEEE Conference on Computer Vision and Pattern Recognition (CVPR)*, pp. 1597–1604, 2009.

[20] G. Li and Y. Yu, “Visual saliency based on multiscale deep features,” in *Proceedings of the IEEE Conference on Computer Vision and Pattern Recognition (CVPR)*, 2015.

- [21] W. Luo, Y. Li, R. Urtasun, and R. Zemel, "Understanding the effective receptive field in deep convolutional neural networks," in *Proceedings of the Advances in Neural Information Processing Systems (NeurIPS)*, 2016.
- [22] A. Vaswani, N. Shazeer, N. Parmar, J. Uszkoreit, L. Jones, A. N. Gomez, L. Kaiser, and I. Polosukhin, "Attention is all you need," in *Proceedings of the Advances in Neural Information Processing Systems (NeurIPS)*, 2017.
- [23] R. Ranftl, A. Bochkovskiy, and V. Koltun, "Vision transformers for dense prediction," *arXiv preprint arXiv:2103.13413*, 2021.
- [24] Z. Liu, Y. Lin, Y. Cao, H. Hu, Y. Wei, Z. Zhang, S. Lin, and B. Guo, "Swin transformer: Hierarchical vision transformer using shifted windows," *arXiv preprint arXiv:2103.14030*, 2021.
- [25] B. Wang, Q. Chen, M. Zhou, Z. Zhang, X. Jin, and K. Gai, "Progressive feature polishing network for salient object detection," in *Proceedings of the AAAI Conference on Artificial Intelligence (AAAI)*, pp. 12128–12135, 2020.
- [26] X. Qin, Z. Zhang, C. Huang, C. Gao, M. Dehghan, and M. Jagersand, "Basnet: Boundary-aware salient object detection," in *Proceedings of the IEEE Conference on Computer Vision and Pattern Recognition (CVPR)*, pp. 7479–7489, 2019.
- [27] Y. Pang, X. Zhao, L. Zhang, and H. Lu, "Multi-scale interactive network for salient object detection," in *Proceedings of the IEEE Conference on Computer Vision and Pattern Recognition (CVPR)*, pp. 9413–9422, 2020.
- [28] G. Li, Y. Xie, and L. Lin, "Weakly supervised salient object detection using image labels," in *Proceedings of the AAAI Conference on Artificial Intelligence (AAAI)*, 2018.
- [29] S. Yu, B. Zhang, J. Xiao, and E. G. Lim, "Structure-consistent weakly supervised salient object detection with local saliency coherence," in *Proceedings of the AAAI Conference on Artificial Intelligence (AAAI)*, 2021.
- [30] X. Li, F. Yang, H. Cheng, W. Liu, and D. Shen, "Contour knowledge transfer for salient object detection," in *Proceedings of the European Conference on Computer Vision (ECCV)*, pp. 355–370, 2018.
- [31] D. Zhang, J. Han, and Y. Zhang, "Supervision by fusion: Towards unsupervised learning of deep salient object detector," in *Proceedings of the IEEE International Conference on Computer Vision (ICCV)*, pp. 4048–4056, 2017.
- [32] L. Qu, S. He, J. Zhang, J. Tian, Y. Tang, and Q. Yang, "RGBD salient object detection via deep fusion," *IEEE Transactions on Image Processing (TIP)*, vol. 26, no. 5, pp. 2274–2285, 2017.
- [33] N. Wang and X. Gong, "Adaptive fusion for RGB-D salient object detection," *IEEE Access*, vol. 7, pp. 55277–55284, 2019.
- [34] J. Han, H. Chen, N. Liu, C. Yan, and X. Li, "CNNs-based RGB-D saliency detection via cross-view transfer and multiview fusion," *IEEE transactions on cybernetics*, vol. 48, no. 11, pp. 3171–3183, 2017.
- [35] Y. Piao, Z. Rong, M. Zhang, W. Ren, and H. Lu, "A2dele: Adaptive and attentive depth distiller for efficient RGB-D salient object detection," in *Proceedings of the IEEE Conference on Computer Vision and Pattern Recognition (CVPR)*, pp. 9060–9069, 2020.
- [36] Y. Piao, W. Ji, J. Li, M. Zhang, and H. Lu, "Depth-induced multi-scale recurrent attention network for saliency detection," in *Proceedings of the IEEE International Conference on Computer Vision (ICCV)*, pp. 7254–7263, 2019.
- [37] H. Chen and Y. Li, "Progressively complementarity-aware fusion network for RGB-D salient object detection," in *Proceedings of the IEEE Conference on Computer Vision and Pattern Recognition (CVPR)*, pp. 3051–3060, 2018.
- [38] H. Chen, Y. Li, and D. Su, "Multi-modal fusion network with multi-scale multi-path and cross-modal interactions for RGB-D salient object detection," *Pattern Recognition (PR)*, vol. 86, pp. 376–385, 2019.
- [39] H. Chen and Y. Li, "Three-stream attention-aware network for RGB-D salient object detection," *IEEE Transactions on Image Processing (TIP)*, vol. 28, no. 6, pp. 2825–2835, 2019.
- [40] J.-X. Zhao, Y. Cao, D.-P. Fan, M.-M. Cheng, X.-Y. Li, and L. Zhang, "Contrast prior and fluid pyramid integration for RGBD salient object detection," in *Proceedings of the IEEE Conference on Computer Vision and Pattern Recognition (CVPR)*, pp. 3927–3936, 2019.
- [41] M. Zhang, W. Ren, Y. Piao, Z. Rong, and H. Lu, "Select, supplement and focus for RGB-D saliency detection," in *Proceedings of the IEEE Conference on Computer Vision and Pattern Recognition (CVPR)*, pp. 3472–3481, 2020.
- [42] N. Liu, N. Zhang, and J. Han, "Learning selective self-mutual attention for RGB-D saliency detection," in *Proceedings of the IEEE Conference on Computer Vision and Pattern Recognition (CVPR)*, pp. 13756–13765, 2020.
- [43] W. Ji, J. Li, M. Zhang, Y. Piao, and H. Lu, "Accurate RGB-D salient object detection via collaborative learning," in *Proceedings of the European Conference on Computer Vision (ECCV)*, 2020.
- [44] Y. Pang, L. Zhang, X. Zhao, and H. Lu, "Hierarchical dynamic filtering network for RGB-D salient object detection," in *Proceedings of the European Conference on Computer Vision (ECCV)*, 2020.
- [45] Z. Zhang, Z. Lin, J. Xu, W.-D. Jin, S.-P. Lu, and D.-P. Fan, "Bilateral attention network for RGB-D salient object detection," *IEEE Transactions on Image Processing (TIP)*, vol. 30, pp. 1949–1961, 2021.
- [46] C. Li, R. Cong, Y. Piao, Q. Xu, and C. C. Loy, "RGB-D salient object detection with cross-modality modulation and selection," in *Proceedings of the European Conference on Computer Vision (ECCV)*, pp. 225–241, 2020.
- [47] G. Li, Z. Liu, L. Ye, Y. Wang, and H. Ling, "Cross-modal weighting network for RGB-D salient object detection," in *Proceedings of the European Conference on Computer Vision (ECCV)*, pp. 665–681, 2020.
- [48] A. Luo, X. Li, F. Yang, Z. Jiao, H. Cheng, and S. Lyu, "Cascade graph neural networks for RGB-D salient object detection," in *Proceedings of the European Conference on Computer Vision (ECCV)*, pp. 346–364, 2020.
- [49] S. Chen and Y. Fu, "Progressively guided alternate refinement network for RGB-D salient object detection," in *Proceedings of the European Conference on Computer Vision (ECCV)*, pp. 520–538, 2020.
- [50] M. Zhang, S. X. Fei, J. Liu, S. Xu, Y. Piao, and H. Lu, "Asymmetric two-stream architecture for accurate RGB-D saliency detection," in *Proceedings of the European Conference on Computer Vision (ECCV)*, pp. 374–390, 2020.
- [51] S. Merilaita, N. E. Scott-Samuel, and I. C. Cuthill, "How camouflage works," *Philosophical Transactions of the Royal Society B: Biological Sciences*, vol. 372, no. 1724, p. 20160341, 2017.
- [52] J. Troscianko, J. Skelhorn, and M. Stevens, "Quantifying camouflage: how to predict detectability from appearance," *BMC evolutionary biology*, vol. 17, no. 1, pp. 1–13, 2017.
- [53] T. W. Pike, "Quantifying camouflage and conspicuousness using visual salience," *Methods in Ecology and Evolution*, vol. 9, no. 8, pp. 1883–1895, 2018.
- [54] A. Tankus and Y. Yeshurun, "Convexity-based visual camouflage breaking," *Computer Vision and Image Understanding*, vol. 82, no. 3, pp. 208–237, 2001.
- [55] F. Xue, C. Yong, S. Xu, H. Dong, Y. Luo, and W. Jia, "Camouflage performance analysis and evaluation framework based on features fusion," *Multimedia Tools and Applications*, vol. 75, no. 7, pp. 4065–4082, 2016.
- [56] S. Li, D. Florencio, Y. Zhao, C. Cook, and W. Li, "Foreground detection in camouflaged scenes," in *Proceedings of the IEEE International Conference on Image Processing (ICIP)*, pp. 4247–4251, IEEE, 2017.
- [57] T.-N. Le, T. V. Nguyen, Z. Nie, M.-T. Tran, and A. Sugimoto, "Anabranch network for camouflaged object segmentation," *Computer Vision and Image Understanding*, vol. 184, pp. 45–56, 2019.
- [58] D.-P. Fan, G.-P. Ji, G. Sun, M.-M. Cheng, J. Shen, and L. Shao, "Camouflaged object detection," in *Proceedings of the IEEE Conference on Computer Vision and Pattern Recognition (CVPR)*, pp. 2777–2787, 2020.
- [59] J. Ren, X. Hu, L. Zhu, X. Xu, Y. Xu, W. Wang, Z. Deng, and P.-A. Heng, "Deep texture-aware features for camouflaged object detection," *arXiv preprint arXiv:2102.02996*, 2021.
- [60] B. Dong, M. Zhuge, Y. Wang, H. Bi, and G. Chen, "Towards accurate camouflaged object detection with mixture convolution and interactive fusion," *arXiv preprint arXiv:2101.05687*, 2021.
- [61] N. Carion, F. Massa, G. Synnaeve, N. Usunier, A. Kirillov, and S. Zagoruyko, "End-to-end object detection with transformers," in *Proceedings of the European Conference on Computer Vision (ECCV)*, pp. 213–229, 2020.
- [62] X. Zhu, W. Su, L. Lu, B. Li, X. Wang, and J. Dai, "Deformable DETR: Deformable transformers for end-to-end object detection," in *Proceedings of the The International Conference on Learning Representations (ICLR)*, 2021.
- [63] Z. Dai, B. Cai, Y. Lin, and J. Chen, "UP-DETR: Unsupervised pre-training for object detection with transformers," *Proceedings of the IEEE Conference on Computer Vision and Pattern Recognition (CVPR)*, 2021.
- [64] W. Wang, E. Xie, X. Li, D.-P. Fan, K. Song, D. Liang, T. Lu, P. Luo, and L. Shao, "Pyramid vision transformer: A versatile backbone for dense prediction without convolutions," *arXiv preprint arXiv:2102.12122*, 2021.



- [65] G. Zhang, Z. Luo, K. Cui, and S. Lu, “Meta-DETR: Few-shot object detection via unified image-level meta-learning,” *arXiv preprint arXiv:2103.11731*, 2021.
- [66] S. Zheng, J. Lu, H. Zhao, X. Zhu, Z. Luo, Y. Wang, Y. Fu, J. Feng, T. Xiang, P. H. Torr, and L. Zhang, “Rethinking semantic segmentation from a sequence-to-sequence perspective with transformers,” *Proceedings of the IEEE Conference on Computer Vision and Pattern Recognition (CVPR)*, 2021.
- [67] Y. Xu, Y. Ban, G. Delorme, C. Gan, D. Rus, and X. Alameddine, “TransCenter: Transformers with dense queries for multiple-object tracking,” *arXiv preprint arXiv:2103.15145*, 2021.
- [68] P. Chu, J. Wang, Q. You, H. Ling, and Z. Liu, “Spatial-temporal graph transformer for multiple object tracking,” *arXiv preprint arXiv:2104.00194*, 2021.
- [69] B. Yan, H. Peng, J. Fu, D. Wang, and H. Lu, “Learning spatio-temporal transformer for visual tracking,” *arXiv preprint arXiv:2103.17154*, 2021.
- [70] W. Mao, Y. Ge, C. Shen, Z. Tian, X. Wang, and Z. Wang, “TF-Pose: Direct human pose estimation with transformers,” *arXiv preprint arXiv:2103.15320*, 2021.
- [71] L. Stof, M. Vidal, and A. Mathis, “End-to-End trainable Multi-Instance pose estimation with transformers,” *arXiv preprint arXiv:2103.12115*, 2021.
- [72] S. Jiang, D. Campbell, Y. Lu, H. Li, and R. Hartley, “Learning to estimate hidden motions with global motion aggregation,” *arXiv preprint arXiv:2104.02409*, 2021.
- [73] A. Dosovitskiy, L. Beyer, A. Kolesnikov, D. Weissenborn, X. Zhai, T. Unterthiner, M. Dehghani, M. Minderer, G. Heigold, S. Gelly, J. Uszkoreit, and N. Houlsby, “An image is worth 16x16 words: Transformers for image recognition at scale,” in *Proceedings of the The International Conference on Learning Representations (ICLR)*, 2021.
- [74] K. Han, Y. Wang, H. Chen, X. Chen, J. Guo, Z. Liu, Y. Tang, A. Xiao, C. Xu, Y. Xu, et al., “A survey on visual transformer,” *arXiv preprint arXiv:2012.12556*, 2020.
- [75] Y. Zhang, K. Li, K. Li, L. Wang, B. Zhong, and Y. Fu, “Image super-resolution using very deep residual channel attention networks,” in *Proceedings of the European Conference on Computer Vision (ECCV)*, pp. 286–301, 2018.
- [76] M. Yang, K. Yu, C. Zhang, Z. Li, and K. Yang, “Denseaspp for semantic segmentation in street scenes,” in *Proceedings of the IEEE Conference on Computer Vision and Pattern Recognition (CVPR)*, pp. 3684–3692, 2018.
- [77] Y. Wang, Y. Yang, Z. Yang, L. Zhao, P. Wang, and W. Xu, “Occlusion aware unsupervised learning of optical flow,” in *Proceedings of the IEEE Conference on Computer Vision and Pattern Recognition (CVPR)*, pp. 4884–4893, 2018.
- [78] A. Obukhov, S. Georgoulis, D. Dai, and L. Van Gool, “Gated CRF loss for weakly supervised semantic image segmentation,” in *Proceedings of the Advances in Neural Information Processing Systems (NeurIPS)*, 2019.
- [79] C. Godard, O. Mac Aodha, and G. J. Brostow, “Unsupervised monocular depth estimation with left-right consistency,” in *Proceedings of the IEEE Conference on Computer Vision and Pattern Recognition (CVPR)*, pp. 270–279, 2017.
- [80] T.-Y. Lin, P. Goyal, R. Girshick, K. He, and P. Dollár, “Focal loss for dense object detection,” in *Proceedings of the IEEE International Conference on Computer Vision (ICCV)*, pp. 2980–2988, 2017.
- [81] Q. Yan, L. Xu, J. Shi, and J. Jia, “Hierarchical saliency detection,” in *Proceedings of the IEEE Conference on Computer Vision and Pattern Recognition (CVPR)*, pp. 1155–1162, 2013.
- [82] G. Li and Y. Yu, “Visual saliency based on multiscale deep features,” in *Proceedings of the IEEE Conference on Computer Vision and Pattern Recognition (CVPR)*, pp. 5455–5463, 2015.
- [83] Y. Li, X. Hou, C. Koch, J. M. Rehg, and A. L. Yuille, “The secrets of salient object segmentation,” in *Proceedings of the IEEE Conference on Computer Vision and Pattern Recognition (CVPR)*, pp. 280–287, 2014.
- [84] V. Movahedi and J. H. Elder, “Design and perceptual validation of performance measures for salient object segmentation,” in *Proceedings of the IEEE Conference on Computer Vision and Pattern Recognition Workshops (CVPRW)*, pp. 49–56, 2010.
- [85] J.-J. Liu, Q. Hou, M.-M. Cheng, J. Feng, and J. Jiang, “A simple pooling-based design for real-time salient object detection,” in *Proceedings of the IEEE Conference on Computer Vision and Pattern Recognition (CVPR)*, pp. 3917–3926, 2019.
- [86] X. Qin, Z. Zhang, C. Huang, C. Gao, M. Dehghan, and M. Jagersand, “BASNet: Boundary-aware salient object detection,” in *Proceedings of the IEEE Conference on Computer Vision and Pattern Recognition (CVPR)*, pp. 7479–7489, 2019.
- [87] J.-X. Zhao, J.-J. Liu, D.-P. Fan, Y. Cao, J. Yang, and M.-M. Cheng, “EGNet: edge guidance network for salient object detection,” in *Proceedings of the IEEE International Conference on Computer Vision (ICCV)*, pp. 8779–8788, 2019.
- [88] H. Zhou, X. Xie, J.-H. Lai, Z. Chen, and L. Yang, “Interactive two-stream decoder for accurate and fast saliency detection,” in *Proceedings of the IEEE Conference on Computer Vision and Pattern Recognition (CVPR)*, pp. 9141–9150, 2020.
- [89] P. Skurowski, H. Abdulameer, J. Błaszczczyk, T. Depta, A. Kornacki, and P. Koziel, “Animal camouflage analysis: Chameleon database,” in *Unpublished Manuscript*, 2018.
- [90] Y. Lv, J. Zhang, Y. Dai, A. Li, B. Liu, N. Barnes, and D.-P. Fan, “Simultaneously localize, segment and rank the camouflaged objects,” in *Proceedings of the IEEE Conference on Computer Vision and Pattern Recognition (CVPR)*, 2021.
- [91] R. Ju, Y. Liu, T. Ren, L. Ge, and G. Wu, “Depth-aware salient object detection using anisotropic center-surround difference,” *Signal Processing: Image Communication*, vol. 38, pp. 115 – 126, 2015.
- [92] H. Peng, B. Li, W. Xiong, W. Hu, and R. Ji, “RGBD salient object detection: A benchmark and algorithms,” in *Proceedings of the European Conference on Computer Vision (ECCV)*, pp. 92–109, 2014.
- [93] N. Li, J. Ye, Y. Ji, H. Ling, and J. Yu, “Saliency detection on light field,” in *Proceedings of the IEEE Conference on Computer Vision and Pattern Recognition (CVPR)*, pp. 2806–2813, 2014.
- [94] Y. Cheng, H. Fu, X. Wei, J. Xiao, and X. Cao, “Depth enhanced saliency detection method,” in *Proceedings of international conference on internet multimedia computing and service*, pp. 23–27, 2014.
- [95] Y. Niu, Y. Geng, X. Li, and F. Liu, “Leveraging stereopsis for saliency analysis,” in *Proceedings of the IEEE Conference on Computer Vision and Pattern Recognition (CVPR)*, pp. 454–461, 2012.
- [96] D.-P. Fan, Z. Lin, Z. Zhang, M. Zhu, and M.-M. Cheng, “Rethinking RGB-D Salient Object Detection: Models, Datasets, and Large-Scale Benchmarks,” *IEEE Transactions on neural networks and learning systems*, 2020.
- [97] D.-P. Fan, C. Gong, Y. Cao, B. Ren, M.-M. Cheng, and A. Borji, “Enhanced-alignment measure for binary foreground map evaluation,” *Proceedings of the International Joint Conferences on Artificial Intelligence (IJCAI)*, pp. 698–704, 2018.
- [98] D.-P. Fan, M.-M. Cheng, Y. Liu, T. Li, and A. Borji, “Structure-measure: A new way to evaluate foreground maps,” in *Proceedings of the IEEE International Conference on Computer Vision (ICCV)*, pp. 4548–4557, 2017.
- [99] J. Deng, W. Dong, R. Socher, L.-J. Li, K. Li, and L. Fei-Fei, “Imagenet: A large-scale hierarchical image database,” in *Proceedings of the IEEE Conference on Computer Vision and Pattern Recognition (CVPR)*, pp. 248–255, 2009.
- [100] S.-H. Gao, Y.-Q. Tan, M.-M. Cheng, C. Lu, Y. Chen, and S. Yan, “Highly efficient salient object detection with 100k parameters,” in *Proceedings of the European Conference on Computer Vision (ECCV)*, pp. 702–721, 2020.
- [101] A. Li, J. Zhang, Y. Lv, B. Liu, T. Zhang, and Y. Dai, “Uncertainty-aware joint salient object and camouflaged object detection,” in *Proceedings of the IEEE Conference on Computer Vision and Pattern Recognition (CVPR)*, 2021.
- [102] Q. Zhai, X. Li, F. Yang, C. Chen, H. Cheng, and D.-P. Fan, “Mutual graph learning for camouflaged object detection,” in *Proceedings of the IEEE Conference on Computer Vision and Pattern Recognition (CVPR)*, 2021.
- [103] H. Mei, G.-P. Ji, Z. Wei, X. Yang, X. Wei, and D.-P. Fan, “Camouflaged object segmentation with distraction mining,” in *Proceedings of the IEEE Conference on Computer Vision and Pattern Recognition (CVPR)*, vol. 1, 2021.
- [104] D.-P. Fan, G.-P. Ji, T. Zhou, G. Chen, H. Fu, J. Shen, and L. Shao, “Pranet: Parallel reverse attention network for polyp segmentation,” in *International Conference on Medical Image Computing and Computer-Assisted Intervention*, pp. 263–273, Springer, 2020.
- [105] D.-P. Fan, G.-P. Ji, M.-M. Cheng, and L. Shao, “Concealed object detection,” *arXiv preprint arXiv:2102.10274*, 2021.
- [106] K. Fu, D.-P. Fan, G.-P. Ji, and Q. Zhao, “JL-DCF: Joint learning and densely-cooperative fusion framework for RGB-D salient object detection,” in *Proceedings of the IEEE Conference on Computer Vision and Pattern Recognition (CVPR)*, pp. 3052–3062, 2020.
- [107] M. Naseer, K. Ranasinghe, S. Khan, M. Hayat, F. S. Khan, and M.-H. Yang, “Intriguing properties of vision transformers,” *arXiv preprint arXiv:2105.10497*, 2021.

- [108] X. Chen, S. Xie, and K. He, “An empirical study of training self-supervised vision transformers,” *arXiv preprint arXiv:2104.02057*, 2021.
- [109] J. Liu, J. Zhang, and N. Barnes, “Confidence-aware learning for camouflaged object detection,” *arXiv preprint arXiv:2106.11641*, 2021.
- [110] K. Zhang, W. Luo, Y. Zhong, L. Ma, W. Liu, and H. Li, “Adversarial spatio-temporal learning for video deblurring,” *IEEE Transactions on Image Processing (TIP)*, vol. 28, no. 1, pp. 291–301, 2018.
- [111] J. Liu, J. Zhang, Y. Hong, and N. Barnes, “Learning structure-aware semantic segmentation with image-level supervision,” in *International Joint Conference on Neural Networks (IJCNN)*, 2021.
- [112] T. Takikawa, D. Acuna, V. Jampani, and S. Fidler, “Gated-scnn: Gated shape cnns for semantic segmentation,” in *ICCV*, 2019.
- [113] M. A. Islam, M. Kalash, and N. D. Bruce, “Revisiting salient object detection: Simultaneous detection, ranking, and subitizing of multiple salient objects,” in *Proceedings of the IEEE Conference on Computer Vision and Pattern Recognition (CVPR)*, pp. 7142–7150, 2018.
- [114] K. Zhang, W. Luo, W. Ren, J. Wang, F. Zhao, L. Ma, and H. Li, “Beyond monocular deraining: Stereo image deraining via semantic understanding,” in *Proceedings of the European Conference on Computer Vision (ECCV)*, pp. 71–89, 2020.
- [115] K. Zhang, W. Luo, Y. Zhong, L. Ma, B. Stenger, W. Liu, and H. Li, “Deblurring by realistic blurring,” in *Proceedings of the IEEE Conference on Computer Vision and Pattern Recognition (CVPR)*, pp. 2737–2746, 2020.